Liquid Crystals
Publication details, including instructions for authors and subscription information:
http://www.informaworld.com/smpp/title~content=t713926090

Modelling of microstructure in mesophases

S. E. Bedford[ab]; A. H. Windle[a]
[a] Department of Materials Science and Metallurgy, University of Cambridge, Cambridge, England [b] Unilever Research, Port Sunlight Laboratory, England

To cite this Article Bedford, S. E. and Windle, A. H.(1993) 'Modelling of microstructure in mesophases', Liquid Crystals, 15: 1, 31 — 63
To link to this Article: DOI: 10.1080/02678299308027838
URL: http://dx.doi.org/10.1080/02678299308027838

LIQUID CRYSTALS, 1993, VOL. 15, NO. 1, 31–63

Modelling of microstructure in mesophases

by S. E. BEDFORD† and A. H. WINDLE*

Department of Materials Science and Metallurgy, University of Cambridge, Pembroke Street, Cambridge CB2 3QZ, England

(*Received 4 August 1992; accepted 6 January 1993*)

Small-molecule liquid crystals show textures which are readily studied at low magnification in the optical polarizing microscope. In polymeric liquid crystals, however, the textures are often much finer, taxing the microscope's resolution. Nevertheless, studies of microstructure in such polymers have been made and it is apparent that they can differ widely both from small-molecule liquid crystals and, indeed, from polymer to polymer. This paper sets out to account for these variations by exploring the effect on microstructure of the marked differences between the magnitudes of the splay, twist and bend elastic constants which are a characteristic of many liquid crystalline polymers. We report a computer model which simulates the development of microstructure for different ratios of the elastic constants. When these are approximately equal, textures characteristic of small-molecule liquid crystals result, such as those involving escape into the third dimension with the degeneration of line defects into points. When the splay energy is high in comparison with bend and twist, as is the case for many thermotropic liquid crystalline copolyesters, escape does not occur and half integral disclination lines predominate. For simulations involving planar boundary conditions, layered microstructures result, frequently with little matching of the orientation from layer to layer. Within the layers the trajectory of the orienting units is sinuous. This simulated microstructure resembles textures observed in thermotropic copolyesters, studied both in this laboratory and elsewhere. The computer model uses a lattice approach which is similar in some respects to that developed by Lebwohl and Lasher. It should not be thought of as a molecular scale model, however, but rather as one based on assemblies of molecules which share a common director.

1. Introduction

The patterns of defects, or texture, apparent when a small-molecule nematic liquid crystal is observed in the polarizing microscope have been studied for almost a century [1] and many of their features are now well-characterized [2]. Although some of these textures occur in polymeric as well as small-molecule liquid crystals, the interpretation of microstructure in polymeric mesophases still presents many challenges, since it often occurs at a scale approaching the resolution limit of the optical microscope. In addition, many of the textures of liquid crystalline polymers vary both from those in small-molecule liquid crystals and also from each other. For example, random copolyesters [3] may exhibit microstructures which appear as a fine speckle and which, although mobile, do not appear to coarsen with time, while polymers containing flexible spacers in the main chain show microstructures that relax to a more conventional threaded texture [4].

* Author for correspondence.

† Present address: Unilever Research, Port Sunlight Laboratory, Bebington, Wirral, England.

0267–8292/93 $10·00

The driving force for the development of specific microstructures in liquid crystalline polymers is the minimization of the elastic distortion energy comprising splay, twist and bend components (K_1, K_2 and K_3, respectively) [5]. Of the various cross terms which are only non-negligible at large distortions, and depend on the second derivatives of the director, K_{13} is likely to be the most significant. However, while we have neglected this parameter in this study, we are aware that some corrections may be necessary to the predicted director distributions in regions of severe distortion such as disclination cores. For thermotropic main chain polymers, the highest energy component is most usually splay [6], while for lyotropic main chain and smectic side chain polymers bend may be the largest. We have developed a model that simulates the evolution of microstructure as the material is, in effect, annealed isothermally in the nematic phase, while at the same time permitting study of the influence of particular disparities in the magnitudes of the three elastic constants. It is thus possible to carry out microstructural simulations of both polymeric and small-molecule mesophases. This model has been described previously for the case of 2/2 dimensions and equal elastic constants [7] and is extended here to include more general three dimensional structures and disparate values of the elastic constants.

The model consists of a lattice of directors, represented by unit vectors, whose centres are fixed on the sites of a primitive cubic lattice while their orientations are allowed to vary in three dimensions. Annealing is simulated by minimizing the energy of a given director with respect to its nearest neighbours. This approach shares many similarities with that initiated by Lebwohl and Lasher [8] and developed by Allen and Wilson [9] and Denham and co-workers [10]. An important difference, however, is that those models are approximately molecular in scale, while the model described here is supramolecular, describing ordering and thus microstructures over much greater distances than would be possible using existing molecular modelling techniques. This microstructural model forms a bridge between molecular modelling and the simulation of observed properties.

It has previously been shown [7] that the interaction potential between two cells can be modelled as the square of the sine of the angle between their directors. When the elastic constants are equal this potential is reduced, for small angles, to a simple average of the orientations with respect to some arbitrary axis. This 'averaging algorithm' is very efficient computationally but is not valid when the elastic constants are not equal and so, for consistency, it is not used in any of the simulations described in this paper.

We have considered three different constraining lattices. 2/2 dimensional simulations are defined as those based on a square lattice containing N^2 cells, in which all the vectors are constrained to lie in the same plane, the term 2/2 thus implying that the directors are free to rotate in two dimensions in the plane of a two dimensional model. In simulations termed 2/3 dimensional, the vectors are again confined to a plane, but this time the lattice is three dimensional cubic, containing N^3 cells. Both of these lattices simulate planar textures. In order to model more general structures, the model is extended into 3/3 dimensions by using a cubic lattice and allowing the vectors complete rotational freedom.

It is also important to address the issue as to the degree to which the algorithm, which is essentially an iterative method for the three dimensional solution of the Frank equations, provides a useful model of the relaxation processes observed in liquid crystalline microstructures. In [7], account is given of the effect of reorienting the central director of any cell group visited through only a small proportion of the angle required to reach the minimum energy position. It was found that, beyond slowing the

computational process, it had little effect on the nature of the microstructures seen during different stages of the relaxation sequence. The algorithm is thus considered as having a first order capability to model the development of a microstructure, and several of the structures to be discussed below do not represent a final, minimum energy state, but intermediate developments which are none the less especially relevant to polymers in which structures are typically non-equilibrium, being limited kinetically. Further refinements of the modelling sequence, in which orientation adjustments are made on a fine scale and limited to favourable local energy gradients, are currently being introduced into the algorithms and will feature in future publications.

2. 2/2 Dimensional simulations

The relaxation algorithm for 2/2 dimensional simulations has been discussed briefly in a previous paper [7], but it is useful to outline it again as a logical introduction to the more refined treatment which enables the three elastic constants to be handled separately. It should also be emphasized that while 2/2 dimensional simulations are particularly simple, and demonstrate the development of long range orientational order in the absence of Brownian motion (i.e. at 0 K), genuine long range orientational order does not occur in such systems at finite temperatures [10].

In general, the starting point for the simulations is the isotropic phase, in which all the directors are randomly oriented except for those within the edge cells which are set to specific orientations to represent periodic, free or fixed boundary conditions as required. Microstructural development proceeds by picking a cell at random and calculating the minimum energy position for its given environment of nearest neighbours. The chosen vector then moves to this minimum position. Another cell is then picked at random and the process repeated. After a given number of cycles, the simulated microstructure is plotted and the process continued until no further reduction in the total energy of the lattice is achieved.

The interaction potential can be illustrated by considering the possible rotations of two isolated rigid rods fixed with respect to their centres of gravity. Stable equilibrium is achieved when the two rods are either parallel or antiparallel while unstable equilibrium corresponds to the orthogonal positions. An energy function which has been used by previous workers [9], and which has been shown to be a good approximation to more rigorous derivations [11], is $\sin^2(\theta-\phi)$, where θ and ϕ are the angles made by the rods in the respective cells to an external reference direction. In 2/2 dimensional simulations, the simplest treatment using a square lattice means that the contribution to the total energy of the structure due to one particular cell can be taken as the sum of the interaction energy over the cell's four nearest neighbours. For the cell shown in figure 1, in which the orientation of the central cell is ϕ and that of each neighbour is θ_i, the energy is given by

$$E=\sum_{i=1}^{4}\sin^2(\theta_i-\phi), \tag{1}$$

and the best orientation of the central cell, ϕ_{opt}, is found by differentiating this expression with respect to ϕ and rearranging to give

$$\tan 2\phi_{\text{opt}}=\frac{\sum_{i=1}^{4}\sin 2\theta_i}{\sum_{i=1}^{4}\cos 2\theta_i}. \tag{2}$$

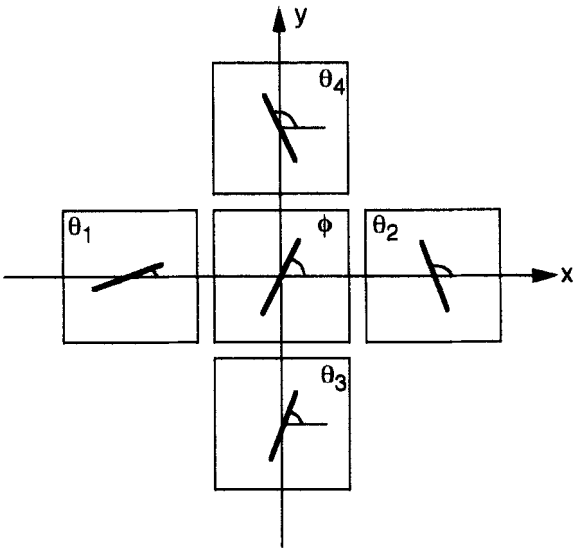

Figure 1. Definition of the angles used to calculate the interaction energy in equation (1).

From the shape of the tan 2θ curve it can be seen that there are two possible solutions for ϕ_{opt} occurring between 0° and 180°, corresponding to minimum and maximum energy orientations. These are substituted back into the original energy expression and the lower energy solution chosen.

Expressions (1) and (2) have been derived for materials in which the elastic constants are assumed equal and set to unity. This approximation, which is not unreasonable for small-molecule liquid crystals where the elastic constants do not differ greatly, is not readily applicable to thermotropic liquid crystalline polymers in which the splay constant is usually higher than that of bend and twist [5]. The next step is therefore to develop expression (1) to account separately for the different modes of distortion.

2.1. *The splay and bend weighting*

In 2/2 dimensions, the only possible distortions are splay or bend or combinations of these, and their separate influences can be seen by examining the central row of cells in figure 2 (*a*). The left hand cell in which the director orientation, denoted by θ_1, is horizontal is held, at this initial stage, to have only a bend influence on the central cell irrespective of the central director orientation ϕ. In contrast, the right hand cell in which the director, θ_2, is vertical has only a splay influence on the central cell. If, however, the director of either of these neighbouring cells is at some arbitrary angle, as shown in figure 2 (*b*), then it will influence the central director through both splay and bend components, appropriately weighted. For neighbours one and two in figure 2 (*b*), this weighting is given by the relationship

$$BE\cos^2\theta_i + SP\sin^2\theta_i, \tag{3}$$

where $i = 1$ or 2. This expression has the appropriate bounding conditions of pure splay when $\theta_i = 90°$ and pure bend when $\theta_i = 0$ (as measured from the x axis), together with a value of unity for all angles when $SP = BE$. The coefficients SP and BE are used in expression (5) rather than K_1 and K_3 respectively, because it is the ratio of splay to bend

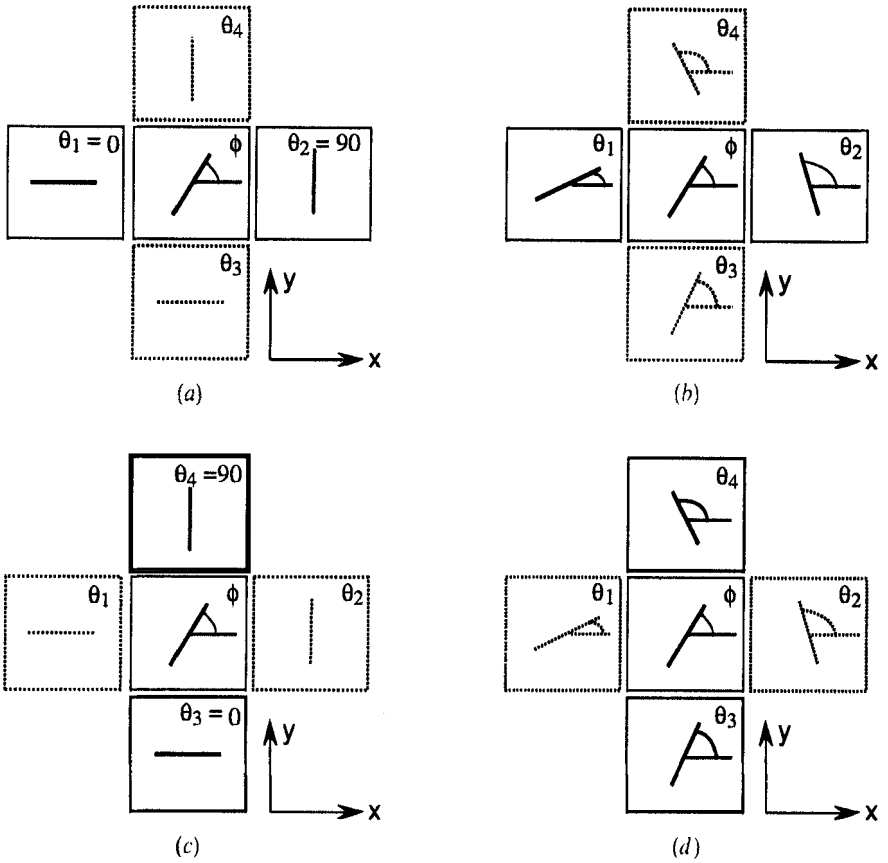

Figure 2. (*a*) Two dimensional lattice considering only the middle row of directors. $\theta_1 = 0$ influences the director only through bend, while $\theta_2 = 90$ influences the director only through splay. In (*b*) θ_1, and θ_2 have arbitrary orientation and interact with the central cell through both splay and bend as given in expression (3). In (*c*) $\theta_3 = 0$ influences the central director through splay and $\theta_4 = 90$ bend. The arbitrary θ_3 and θ_4 in (*d*) interact through both splay and bend as described by expression (4).

energy that is important in the expression rather than their absolute magnitudes. For example, if $K_1 = 5 \times 10^{-7}$ dyne and $K_3 = 10{\cdot}1 \times 10^{-7}$ dyne, values for the small-molecule liquid crystal PAA at 120°C [12], $SP = 1$ and $BE = 2{\cdot}02$.

In figures 2(*c*) and (*d*), the splay and bend influences down a column of cells are established. It can be seen that the mode of distortion is reversed with respect to the row of cells, so that in figure 2(*c*) there is only a splay influence from cell three and a bend influence from cell four. Therefore, for arbitrary angles θ_i, the weighting is now given by

$$SP \cos^2 \theta_i + BE \sin^2 \theta_i, \tag{4}$$

where $i = 3$ or 4. In this way the original sine squared energy expression can be weighted by resolving each neighbouring vector into its splay and bend components. For the lattice shown in figure 1

$$E = \sum_{i=1}^{2} (BE \cos^2 \theta_i + SP \sin^2 \theta_i) \sin^2 (\theta_i - \phi) + \sum_{i=3}^{4} (BE \sin^2 \theta_i + SP \cos^2 \theta_i) \sin^2 (\theta_i - \phi), \tag{5}$$

and energy minimization to find the optimum ϕ gives

$$\tan 2\phi_{opt} = \frac{\sum_{i=1}^{2} (BE\cos^2\theta_i + SP\sin^2\theta_i)\sin 2\theta_i + \sum_{i=3}^{4} (BE\sin^2\theta_i + SP\cos^2\theta_i)\sin 2\theta_i}{\sum_{i=1}^{2} (BE\cos^2\theta_i + SP\sin^2\theta_i)\cos 2\theta_i + \sum_{i=3}^{4} (BE\sin^2\theta_i + SP\cos^2\theta_i)\cos 2\theta_i}, \quad (6)$$

so that the process of microstructural development by energy minimization can be followed as before using the modified expression.

These splay and bend weightings are in accord with Frank's definition of the splay and bend distortions when applied to a two dimensional lattice. From the Frank definitions [13]

splay: $$s_1 = \frac{\partial n_x}{\partial x'}, \qquad s_2 = \frac{\partial n_y}{\partial y'}, \quad (7)$$

bend: $$b_1 = \frac{\partial n_x}{\partial y'}, \qquad b_2 = \frac{\partial n_y}{\partial x'}, \quad (8)$$

where s_1 and s_2 are the components of splay, b_1 and b_2 are the components of bend and ∂n_x, and ∂n_y the components of the director in the x and y directions. Therefore, in the lattice shown in figure 2, along a row (the x direction), splay is a maximum for $x_i = 0$ as in cell 2, while bend is a maximum for $y_i = 0$ as in cell 1, and down a column (the y direction) the mode of distortion is reversed.

As an example of the use of expressions (5) and (6), consider the row of cells in figure 3(*a*). $\theta_1 = 0°$, $\theta_2 = 45°$ and ϕ_{opt}, the orientation of the central cell, remains to be determined. From expression (5) the total energy, E, of the row is given by

$$E = (BE\cos^2 0° + SP\sin^2 0°)\sin^2(0° - \phi) + (BE\cos^2 45° + SP\sin^2 45°)\sin^2(45° - \phi), \quad (9)$$

which is plotted agains the angle, ϕ, for three different ratios of the elastic constants in figure 3(*b*). The figure shows that the optimum angle of the central cell, ϕ_{opt}, corresponding to the minima on the three curves, is different for each of the three elastic constant ratios. These values may be obtained either by reading directly from the plot or by substitution into expression (6) in accordance with the computer algorithm. In either case, the three different values of ϕ_{opt} are (i) 22·5° for $SP = BE$, spreading the defect uniformly between the neighbouring cells, (ii) 45° when $BE = 0$, so that the only distortion is bend and (iii) 13·3° when $SP = 0$, minimizing the amount of bend. These three solutions are sketched in figure 3(*c*).

A potential difficulty is encountered with the model for configurations where the directors are separated by exactly 90°, such as $\theta_1 = 45°$, $\theta_2 = 135°$, $\theta_3 = 135°$ and $\theta_4 = 45°$, because $\tan 2\phi$, as defined by expression (6), is indeterminate. Such exact cases are very unlikely to occur during the simulation, however, and so in practice do not cause a problem.

Before proceeding further we should question whether it is reasonable to assess the level of splay or bend pertaining to the central director as if it is dependent only on the orientation of the surrounding directors. Look again at figure 2(*a*). While the influence of the director of cell 1 on the central cell will consist only of bend, the effect of the orientation of the central director on cell 1 will be a combination of both splay and bend, in view of the arbitrary value of ϕ chosen in the diagram. It is thus unreasonable to assume that the distortion field resulting from the relative orientations of the two

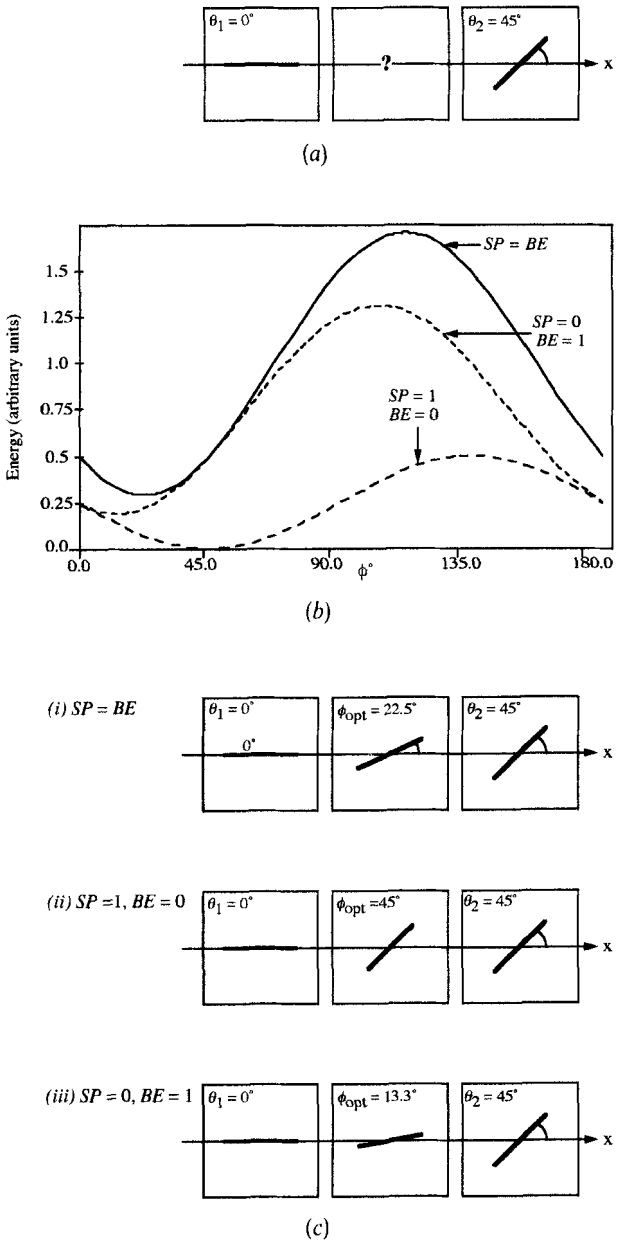

Figure 3. Example of the algorithm for a row of three cells in two dimensions. In (*a*) $\theta_1 = 0$, $\theta_2 = 45$ and the orientation of the central cell, ϕ, is to be determined. In (*b*) the total energy of the central cell is calculated in accordance with expression (5) for three limiting ratios of the elastic constants. The three values of ϕ_{opt}, corresponding to the three elastic constant ratios are given in (*c*).

directors will be pure bend. We have therefore extended the expressions (3) and (4), the weighting of distortion field types, so that they take into account the orientation of the central director on an equal basis to that of each of the surrounding directors. Hence the expressions (3) and (4) become, respectively

$$0{\cdot}5(BE\cos^2\theta_i + SP\sin^2\theta_i) + 0{\cdot}5(BE\cos^2\phi + SP\sin^2\phi), \tag{10}$$

$$0{\cdot}5(SP\cos^2\theta_i + BE\sin^2\theta_i) + 0{\cdot}5(SP\cos^2\phi + BE\sin^2\phi), \tag{11}$$

while the relation for the energy in expression (5) becomes

$$E = 0{\cdot}5\sum_{i=1}^{2}((BE(\cos^2\theta_i + \cos^2\phi) + SP(\sin^2\theta_i + \sin^2\phi))\sin^2(\theta_i - \phi))$$

$$+ 0{\cdot}5\sum_{i=3}^{4}((SP(\cos^2\theta_i + \cos^2\phi) + BE(\sin^2\theta_i + \sin^2\phi))\sin^2(\theta_i - \phi)). \tag{12}$$

The increased algebraic complexity of these more realistic equations has led us to adopt a different approach to the determination of the minimum energy value of ϕ. For although expression (12) can be readily differentiated, as could expression (5), the next step, which involves the extension of the treatment to 3/3 dimensions, yields equations which are distinctly unwieldy. While this work is recorded elsewhere [14], it is not developed here, as the alternative iterative approach to the minimization of E_ϕ has proved much more robust in the more complex situations treated below. For the iterative method, the director of the central cell is rotated through a completely random angle to a trial position and its new energy computed. If this is less than was achieved at any previous settings it is accepted. This approach is especially versatile as it permits simulations at finite temperatures for levels of structure in which each cell contains at most a small group of molecules. Temperature dependent modelling is achieved where the acceptance or rejection of a given trial orientation is set to be exponentially dependent on the ratio of its energy to the absolute temperature. The modelling of larger scale microstructures reported here is equivalent to 0 K and so only the orientation with the lowest value of E_ϕ is accepted. As the equilibrium structure is approached, this algorithm becomes rather sluggish, since few tries are accepted. The speed of convergence is enhanced at this point by using, as the simulation develops, progressively smaller random increments in orientation with respect to the previous setting. This method is described more fully by Allen and Tildesley [15].

In the case where the energy constants are equal, equation (12) reduces to (5), and thus the simulation behaviour is equivalent. However, where splay energy is set to be much larger than bend, or vice versa, the use of the modified term for energy in expression (12) avoids the phenomenon of lattice 'print through' where the energy distribution within a director field, such as that around a disclination, depends to some extent on the orientation of the director in relation to the cell axes.

2.2. *Performance of the model with discrete splay and bend elastic coefficients*

In this section some examples of the model are described for a square lattice of cells. This intermediate step is introduced in order to test that the model behaves correctly in 2/2 dimensions before moving on to the more physically realistic, but computationally demanding 3/3 dimensional case. Using a Vax 3100, the simulation of microstructural development, from the totally random isotropic phase through to the ordered monodomain, requires approximately 5 min of computing time for a lattice of 35×35 cells. This speed is a reflection of the straightforward energy expression and the

relatively small number of cells. The microstructures selected, and if necessary forced on the simulation through the choice of appropriate boundary conditions, were examples of $s = \pm 1$ and $s = \pm \frac{1}{2}$ disclinations. The trajectory patterns of these disclinations are well-known, both where the elastic constants are the same and where they are different [16, 17]. It is thus possible to compare readily the simulated and analytically derived structures.

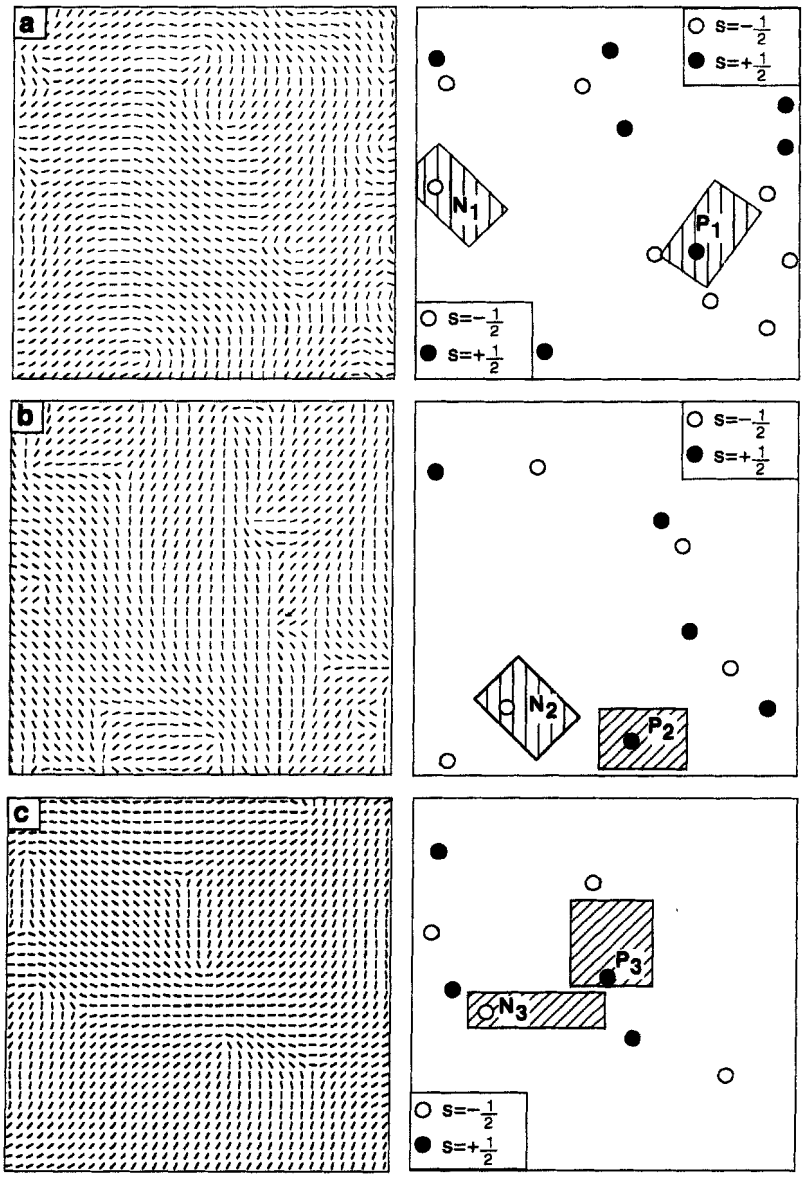

Figure 4. Typical examples of simulated two dimensional microstructures using free boundary conditions, together with schematic plots of the coordinates of the $s = +\frac{1}{2}$ and $s = -\frac{1}{2}$ disclination cores. The simulations are based on relation (12) and are thus free from print through. The values of ε are (*a*) −0·98, (*b*) 0·98, (*c*) 0·0, representing high splay, high bend, and equal splay and bend energies respectively.

2.2.1. *Simulation of* $s=\frac{1}{2}$ *disclinations with discrete elastic constants*

$s=\pm\frac{1}{2}$ disclinations are energetically favourable in 2/2 dimensions because the energy of a disclination varies as the square of its strength. As a result, this disclination type predominates in two dimensional simulations, irrespective of whether the elastic constants are equal or different. Figure 4 shows typical examples of simulated two dimensional microstructures, together with schematic 'disclination maps' that plot the coordinates of the $s=+\frac{1}{2}$ and $s=-\frac{1}{2}$ disclination cores in each case. They have all been obtained for simulations with free boundary conditions and each represents the structure after approximately half the number of iterations required to convert the random starting arrangement into a completely ordered monodomain. In figure 4(*a*) the splay constant is equal to one hundred times that of bend; the fractional difference between the elastic constants, ε, expressed as

$$\varepsilon=\frac{K_3-K_1}{K_3+K_1}, \tag{13}$$

being equal to $-0{\cdot}98$. In figure 4(*b*) the relative magnitude of the elastic constants is reversed so that ε is equal to 0·98, while in figure 4(*c*) the two constants are equal, ε being equal to 0. (ε is sometimes referred to as the elastic anisotropy [16].)

In all 2/2 dimensional simulations, it was observed that there were approximately equal populations of $s=-\frac{1}{2}$ and $s=+\frac{1}{2}$ disclinations, both having the same energy, and that they adopted a spread of orientations in the absence of external fields. The shape of the simulated disclinations did not change as a function of their orientation with respect to the lattice, however, and so could be readily compared for the different values of ε. Comparison of $s=-\frac{1}{2}$ disclinations, whose cores are positioned at N1, N2 and N3, and the $s=+\frac{1}{2}$ disclinations at P1, P2 and P3, shows that the director field surrounding the $s=-\frac{1}{2}$ defects does not alter appreciably with ε, while that of the $s=+\frac{1}{2}$ defects undergoes a considerable change. This marked difference in behaviour can be seen most clearly by reference to the line drawings in figure 5(i) and in figure 6(i) in which continuous lines have been traced over the director patterns from the selected disclinations P1, P2 and P3 and N1, N2 and N3, respectively. The drawings are in the same orientation as the disclinations in the simulated microstructures and the approximate area which has been traced is marked on the disclination maps in figure 4 by hatching. It can be seen that the three $s=+\frac{1}{2}$ defects are associated with very different director trajectories, while the morphology of the $s=-\frac{1}{2}$ defects remains fairly constant, although it is affected slightly by the distorting effect of their neighbouring defects.

The constant morphology of the simulated $s=-\frac{1}{2}$ disclinations, despite variations in ε, is in agreement with the continuum theory which predicts that the symmetry of this defect prevents significant change in structure [18]. It may also be noted that at both extremes of ε, the simulated director field cannot adjust to remove completely the more costly distortion, at least in 2/2 dimensions, and this again is in agreement with theory [18]. The marked morphological variation of $s=+\frac{1}{2}$ disclinations has been observed in nematic liquid crystals using transmission electron microscopy [18] and is also predicted from minimization of the Frank distortion energy expression as described by Nehring and Saupe [16].

In order to determine how closely the shape of the simulated disclinations matches theoretical predictions, director trajectories of both $s=+\frac{1}{2}$ and $s=-\frac{1}{2}$ defects were calculated and are represented in figures 5(ii) and 6(ii). These analytically determined

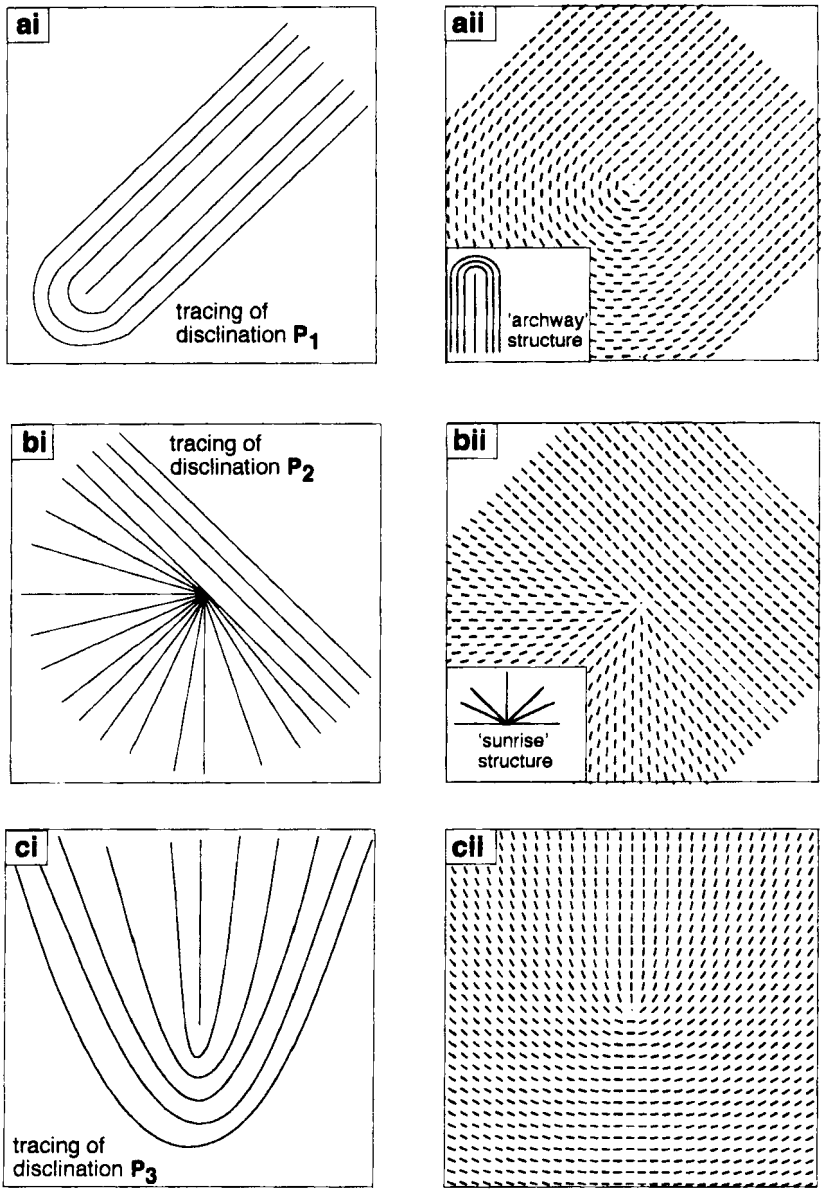

Figure 5. (*a*(i))–(*c*(ii)) Tracings of the $s = +\frac{1}{2}$ disclinations identified by hatching in figure 4. (*a*(ii))–(*c*(ii)) Disclinations with the corresponding elastic anisotropies determined analytically from equation (14). Each of the disclinations is in the same orientation as observed in figure 4. The simulated and calculated structures are in good agreement.

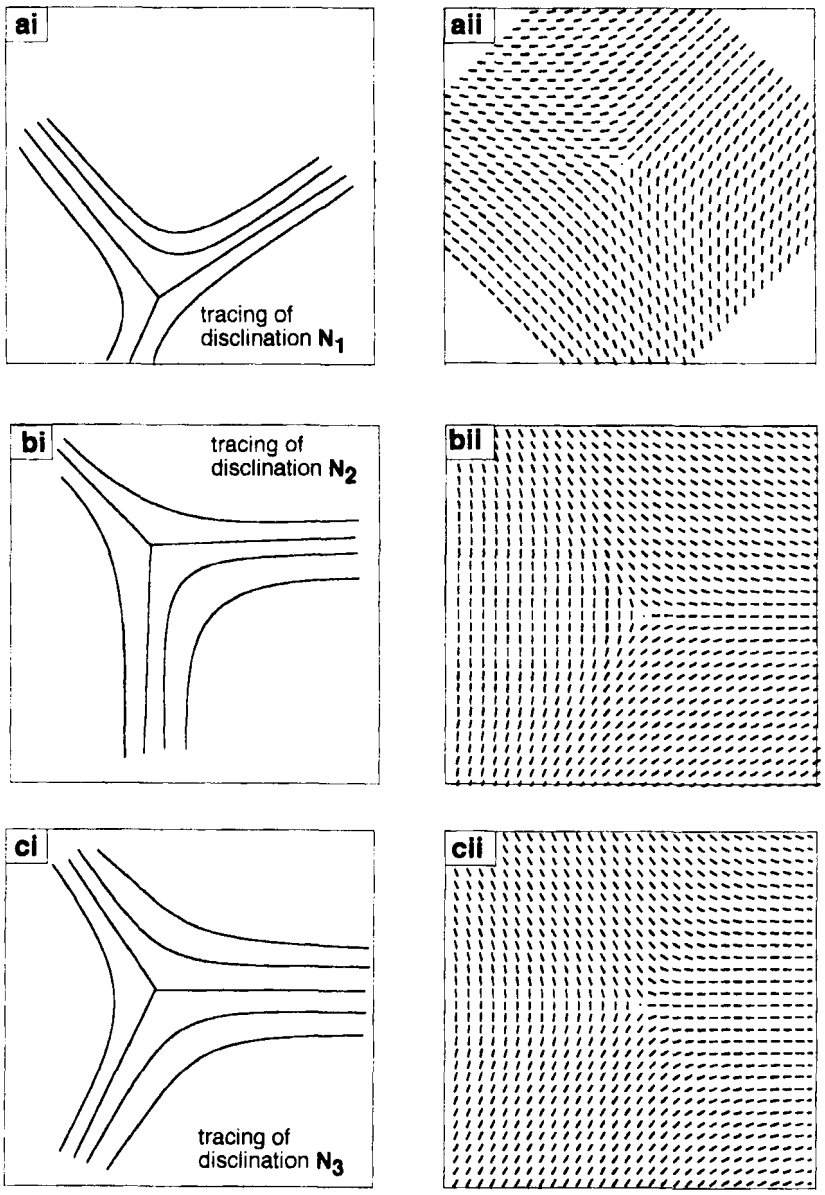

Figure 6. (*a*(i))–(*c*(i)) Tracings of the $s = -\frac{1}{2}$ disclinations shown by hatching in figure 4. (*a*(ii))–(*c*(ii)) disclinations with the same elastic anisotropies as calculated from the continuum theory. Again, all the disclinations are in the same orientations as those in figure 4.

director fields have the same value of ε as the corresponding simulations in figures 5 (i) and 6 (i), but have been obtained by placing vectors onto the lattice in accordance with the expression of Nehring and Saupe [16], a procedure that is similar to that introduced by Nicholson [19]. The calculated patterns are oriented on the page to correspond with those selected from the simulated patterns.

The Nehring and Saupe equation may be expressed as

$$\phi_{\text{disc}} = s\alpha + \varepsilon\left(\frac{s(2-s)}{4(s-1)^2}\right)\sin(2\alpha(s-1)) + C_0, \tag{14}$$

where ϕ_{disc} is the angle the director makes with the x axis at all points along a line which is at an angle, α, to that axis, as defined in figure 7. C_0 is a constant which rotates the disclination, but does not alter its shape, so is set to zero in the calculations.

It can be seen that for each value of ε, the shape of the simulated disclination pattern closely matches the calculated structure. Where $SP = 100$ and $BE = 1$ as in figure 5 (*a*), both the simulated and calculated $s = +\frac{1}{2}$ disclination have a structure resembling that of an archway, containing considerable bend, but very little splay. In figure 5 (*b*), where $SP = 1$ and $BE = 100$, both simulated and calculated structures contain only splay, resembling a sunrise, again shown as an inset. In figure 6, it can be seen that, like the simulated structure, the director trajectory of the $s = -\frac{1}{2}$ disclination calculated from expression (14) undergoes very little change as the ratio of the elastic constants is varied.

It is possible to quantify the extent of similarity between the simulated structures and those given by the Nehring–Saupe expression by measurement of the angles ϕ_{disc} and α as defined in figure 7, for the simulated disclinations, and comparing these values with those expected from the expression. The table shows the results of this comparison for the three $s = +\frac{1}{2}$ disclinations. The theoretical and simulated data match quite closely, although it is difficult to assess the magnitude of the errors which arise from the distorting effect of neighbouring disclinations in the model. Corresponding measurements were not made for the $s = -\frac{1}{2}$ disclinations, because in this case the three morphologies were clearly affected more by the distorting effect of the neighbouring disclinations than by the difference in the elastic constants.

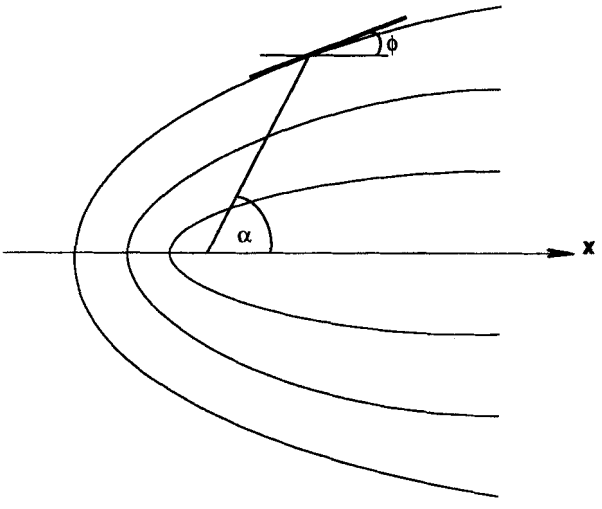

Figure 7. Definition of the angles used to calculate the trajectory of a disclination in the Nehring–Saupe expression.

Comparison of the trajectories of the calculated and simulated $s = +\frac{1}{2}$ disclinations. ϕ_{N-S} is the value of ϕ calculated using the Nehring–Saupe expression and ϕ_m is the value as measured from the simulations.

	α	0	20	40	60	80	100	120	140	160	180
Defect	ϕ_{N-S}	0	−4·7	−7·6	−7·2	−2·3	7·7	22·3	42·4	65·3	90·0
a	ϕ_m	0	0	0	0	0	9·5	25·5	42·0	65·0	90·0
Defect	ϕ_{N-S}	0	24·7	47·6	67·2	82·3	92·4	97·2	96·6	94·6	90·0
b	ϕ_m	0	20·0	40·0	60·0	80·0	90·0	90·0	90·0	90·0	90·0
Defect	ϕ_{N-S}	0	10·0	20·0	30·0	40·0	50·0	60·0	70·0	80·0	90·0
c	ϕ_m	0	10·0	16·0	28·0	40·0	58·0	63·0	68·0	83·0	90·0

2.2.2. *Investigation of* s = *1 disclinations*

Given that the energy of an $s = \pm 1$ disclination is equal to four times that of an $s = \pm\frac{1}{2}$ defect (c.f. §2.2.1), it is to be expected that an $s = +1$ defect would decompose into a pair of $s = +\frac{1}{2}$ defects and likewise an $s = -1$ into two $s = -\frac{1}{2}$ defects. Such decomposition has been modelled for a single $s = +1$ defect placed at the centre of the 2/2 dimensional model. The model was initialized as a plane, radiating field, but was then permitted to run with free (i.e. orientationally unconstrained) boundary conditions and with equal elastic constants. Figure 8 (*a* (i)) shows the initial director field around the defect, while figures 8 (*b* (i)) and (*c* (i)) show the decomposition and repulsion between the two $s = +\frac{1}{2}$ defects as the model relaxes. The two defects would, of course, repel each other out of the model after longer relaxation periods than those shown. Figures 8 (*a* (ii)) to 8 (*c* (ii)) are different presentations of the same structures, the height of the vertical axis being equivalent to the distortion energy within each cell cluster.

The next step is to attempt to force an $s = +1$ defect by fixing the orientations of the boundary cells in accord with the radial director pattern. Figure 9 (*a*) shows that again there are two repelling $s = +\frac{1}{2}$ defects, although in this case the disclinations are retained within the field by the boundary settings irrespective of the number of relaxation iterations. Figure 9 (*b*) shows the effect of introducing a splay energy 100 times that of bend. Not surprisingly, there is no observed propagation of the radial orientation in from the boundaries, where it is set, as such a field is very rich in the splay distortion. However, two $s = +\frac{1}{2}$ disclinations can again be identified. Figure 9 (*c*) is the equivalent model, but with bend now equal to 100 times that of splay. Both the boundary conditions and the relative ease of the splay distortion conspire to give the +1 defect at the centre, although it is perhaps possible to view this defect as two closely spaced $s = \frac{1}{2}$ singularities. (Note that this figure which happened to be calculated using equation (5) rather than the refined version, equation (12), shows some degree of lattice print through, in that the orientations of the directors on a circle drawn within the model do not change orientation completely linearly on moving around that circle.)

3. 2/3 Dimensional simulations

The examples considered in §2 have shown that for both $s = \pm\frac{1}{2}$ and $s = \pm 1$ disclinations, the 2/2 dimensional model behaves correctly, predicting structures which are the same as those which can be calculated analytically (for example, [16]) for such comparatively straightforward geometries. Before moving onto 3/3 dimensional

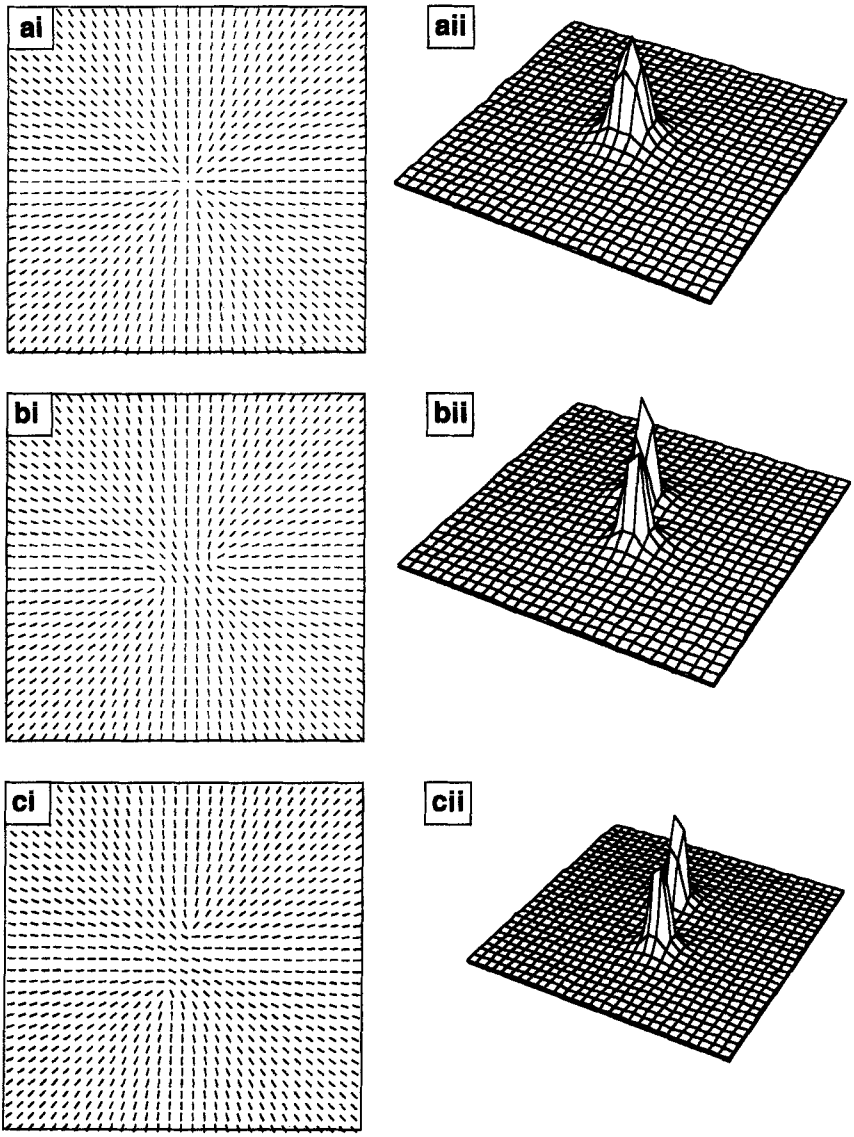

Figure 8. An illustration of the instability of an $s = +1$ disclination in 2/2 dimensions when the elastic constants are equal. (*a* (i)) shows an $s = +1$ radial disclination placed on the lattice. (*b* (i)) The decomposition of the structure into two $s = +\frac{1}{2}$ defects. (*c* (i)) Their mutual repulsion. Figures (*a* (ii))–(*c* (ii)) are a different presentation of the same structures, the height of the vertical axis being equivalent to the distortion energy within each cell cluster.

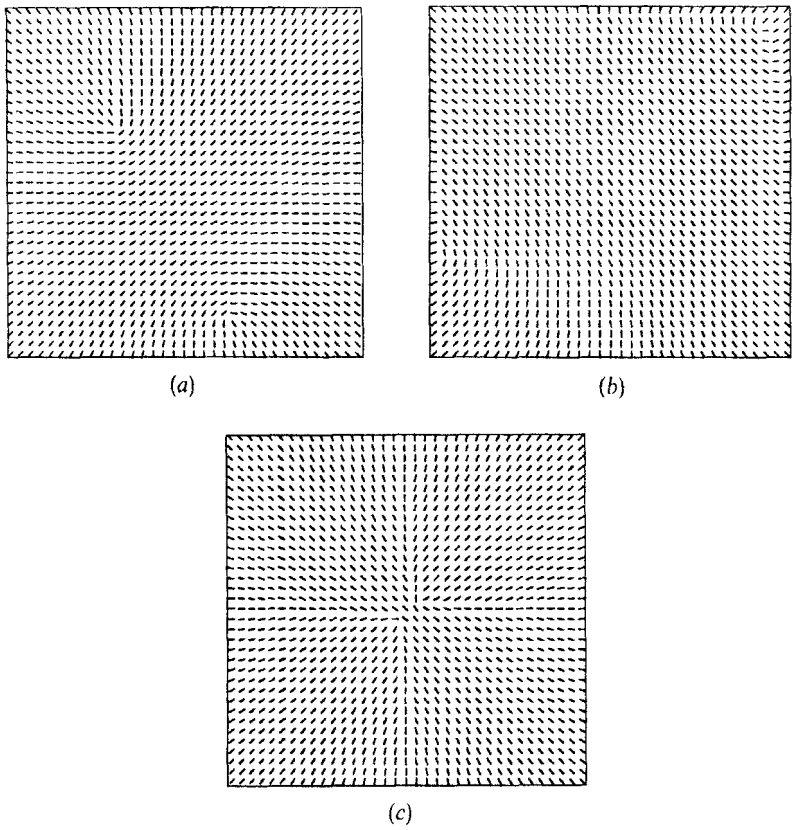

Figure 9. An $s=+1, \eta=0$ disclination simulated using (*a*) $BE=1, SP=1$; (*b*) $SP=100, BE=1$; (*c*) $SP=1, BE=100$. The disclination is only stable in (*c*), forming preferentially $s=+\frac{1}{2}$ disclinations in (*a*) and (*b*). Very close inspection of this figure shows some degree of lattice print through in that the orientations of the directors on a circle drawn within the model do not change uniformly on moving round the circle.

simulations, it is helpful to consider an intermediate, 2/3 dimensional stage as a means of introducing the twist elastic constant.

In these simulations each vector is again confined to lie in the same plane and a cuboid is formed from stacking such planes on top of each other. Within each plane, there exists a combination of splay and bend distortions as before, but there is now an interaction between the central vector and the planes above and below. Since all the vectors are still constrained to lie parallel to the same plane this interaction is pure twist. For the lattice shown in figure 10 the total energy is:

$$E=0{\cdot}5\sum_{i=1}^{2}(BE(\cos^2\theta_i+\cos^2\phi)+SP(\sin^2\theta_i+\sin^2\phi))\sin^2(\theta_i-\phi)$$
$$+0{\cdot}5\sum_{i=3}^{4}(SP(\cos^2\theta_i+\cos^2\phi)+BE(\sin^2\theta_i+\sin^2\phi))\sin^2(\theta_i-\phi)$$
$$+0{\cdot}5\sum_{i=5}^{6}TW\sin^2(\theta_i-\phi), \qquad (15)$$

which may be solved as before to find the optimum orientation of the central cell.

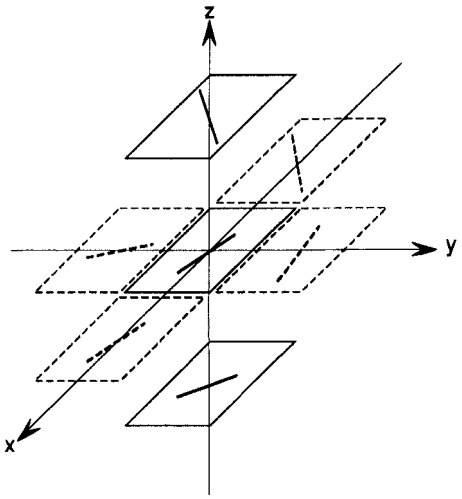

Figure 10. Cell cluster in $2\frac{1}{2}$ dimensions showing the imposed planar constraint.

As an illustration of the twist between layers figure 11 (*a*) shows a stable 'all twist' structure. It has been modelled for equal elastic constants with orthogonal alignment at the top and bottom surfaces and free boundary conditions elsewhere, a geometry reminiscent of that of the twisted nematic cell. The figure comprises orthogonal sections showing both the top surface and two elevations. It may be observed that the twist is uniform and continuous, as expected where the elastic constants are equal [20]. Figure 11 (*b*) shows a similar figure, this time of a microstructure developed where the twist constant is very high compared to that of splay or bend ($TW=100$, $BE=1$ and $SP=1$) and without any fixed boundary condition, in addition to the constraints implied by $2\frac{1}{2}$ dimensions. In order to minimize twist in this case, the model has developed excellent matching of the directors from plane to plane in the z direction, which is most clearly seen from the edge on views. Since the bend and splay elastic constants are very low in comparison, the model, at the stage of relaxation shown, has only poorly developed order within the x–y layers. It should be noted that such structures are highly unlikely in nematic liquid crystals, since in reality, the twist constant is usually lower than that of bend and splay.

4. 3/3 Dimensional simulations

4.1. *The energy potential in three dimensions*

In order to model liquid crystalline structures with greater realism, the simulation must be extended to 3/3 dimensions. Compared with the 2/3 dimensional case, the directors will be able to change orientation in three rather than two dimensions. It has become apparent that for 3/3 dimensions, the algebra is most readily handled in terms of vectors (and thus cartesian coordinates) rather than angles as in the 2/2 dimensional case. When the elastic constants are all set equal to unity, the energy between two neighbouring cells may be expressed as the square of the modulus of the cross product of the two directors. Thus the interaction potential between a central vector, $\mathbf{c}$, and its six neighbouring vectors, $\mathbf{n}_i$, may be written

$$E=\sum_{i=1}^{6}|\mathbf{c}\times\mathbf{n}_i|^2, \tag{16}$$

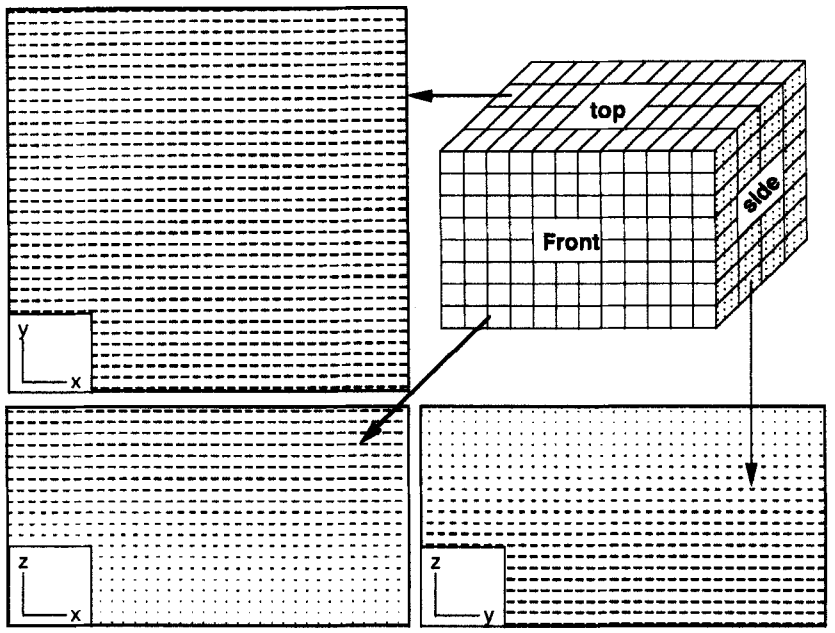

(*a*)

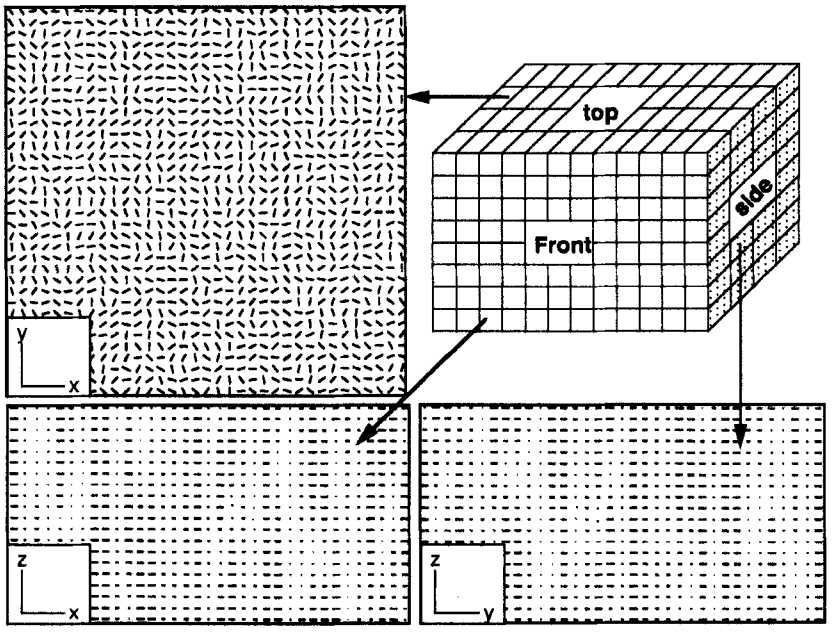

(*b*)

Figure 11. (*a*) A uniform smooth twist developed in a $2\frac{1}{2}$ dimensional lattice for orthogonal boundary conditions on the top and bottom surfaces and equal elastic constants. (*b*) A simulation using free boundary conditions and $SP=1$, $BE=1$ and $TW=100$. There is good matching from layer to layer but little in-layer order.

or, in cartesian coordinates

$$E=\sum_{i=1}^{6}[(x_iy_c-y_ix_c)^2+(y_iz_c-z_iy_c)^2+(z_ix_c-x_iz_c)^2], \tag{17}$$

where x_c, y_c and z_c are the coordinates of the central vector and x_i, y_i and z_i are the coordinates of the neighbouring vectors.

Inclusion of the elastic constants into the energy expression is most conveniently managed in 3/3 dimensions by resolving the vectors onto the three principal orthogonal planes. The energy expressions are then written as the sum of three, two dimensional expressions

On the x–y plane

$$\begin{aligned}E_{xy}=&\frac{1}{2}\sum_{i=1}^{2}\left(BE\left(\left(\frac{y_i}{l_i}\right)^2+\left(\frac{y_c}{l_c}\right)^2\right)+SP\left(\left(\frac{x_i}{l_i}\right)^2+\left(\frac{x_c}{l_c}\right)^2\right)\right)(x_iy_c-y_ix_c)^2 && \text{along } y\\ &+\frac{1}{2}\sum_{i=3}^{4}\left(BE\left(\left(\frac{x_i}{l_i}\right)^2+\left(\frac{x_c}{l_c}\right)^2\right)+SP\left(\left(\frac{y_i}{l_i}\right)^2+\left(\frac{y_c}{l_c}\right)^2\right)\right)(x_iy_c-y_ix_c)^2 && \text{along } x\\ &+\sum_{i=5}^{6}TW(x_iy_c-y_ix_c)^2. && \text{along } z\end{aligned} \tag{18}$$

On the z–x plane

$$\begin{aligned}E_{zx}=&\sum_{i=1}^{2}TW(z_ix_c-x_iz_c)^2 && \text{along } y\\ &+\frac{1}{2}\sum_{i=3}^{4}\left(BE\left(\left(\frac{x_i}{l_i}\right)^2+\left(\frac{x_c}{l_c}\right)^2\right)+SP\left(\left(\frac{z_i}{l_i}\right)^2+\left(\frac{z_c}{l_c}\right)^2\right)\right)(z_ix_c-x_iz_c)^2 && \text{along } x\\ &+\frac{1}{2}\sum_{i=5}^{6}\left(BE\left(\left(\frac{z_i}{l_i}\right)^2+\left(\frac{z_c}{l_c}\right)^2\right)+SP\left(\left(\frac{x_i}{l_i}\right)^2+\left(\frac{x_c}{l_c}\right)^2\right)\right)(z_ix_c-x_iz_c)^2 && \text{along } z\end{aligned} \tag{19}$$

On the y–z plane

$$\begin{aligned}E_{zx}=&\frac{1}{2}\sum_{i=1}^{2}\left(BE\left(\left(\frac{y_i}{l_i}\right)^2+\left(\frac{y_c}{l_c}\right)^2\right)+SP\left(\left(\frac{z_i}{l_i}\right)^2+\left(\frac{z_c}{l_c}\right)^2\right)\right)(y_iz_c-y_iz_c)^2 && \text{along } y\\ &+\sum_{i=3}^{4}TW(y_iz_c-y_iz_c)^2 && \text{along } x\\ &+\frac{1}{2}\sum_{i=5}^{6}\left(BE\left(\left(\frac{z_i}{l_i}\right)^2+\left(\frac{z_c}{l_c}\right)^2\right)+SP\left(\left(\frac{y_i}{l_i}\right)^2+\left(\frac{y_c}{l_c}\right)^2\right)\right)(y_iz_c-y_iz_c)^2, && \text{along } z\end{aligned} \tag{20}$$

where l_i is the length of the projection of the ith neighbouring vector on to each of the planes, and l_c the projected length of the central vector.

The total energy is given by

$$E=E_{xy}+E_{xz}+E_{yz},$$

and it may be noted that when the elastic constants are equal, the relation reduces to expression (17).

4.2. *Performance of the model in 3/3 dimensions*

The remainder of this paper examines the performance of the model in 3/3 dimensions, comparing it where possible with experimentally observed microstructures. Finally, its application in elucidating structures that are not yet fully understood is considered and the scene set for future work.

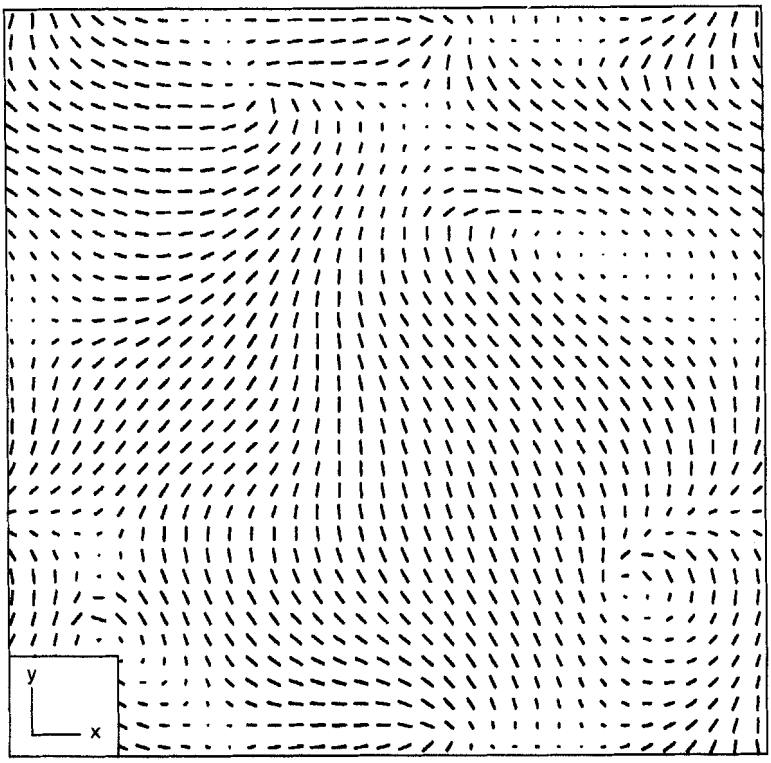

(*a*)

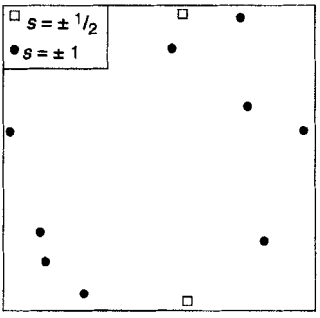

(*b*)

Figure 12. (*a*) x–y section through a $35 \times 35 \times 35$ 3/3 dimensional model simulated using periodic boundary conditions and equal elastic constants. (*b*) A map of the various defects in the structure. It can be seen that many more defects have integral than half integral character as a result of the process 'escape into the third dimension'.

4.2.1. *Point disclinations*

Figure 12 is a slice through a three dimensional structure in which the iterative relaxation has been terminated after approximately half the number of cycles required to produce a monodomain. It is accompanied by a 'disclination map' which replots the approximate positions of the integral and half integral defects. The simulation has been run using periodic boundary conditions and equal elastic constants. The most striking feature is that there appear to be many more $s = \pm 1$ defects than $s = \pm \frac{1}{2}$ defects. However, a single section such as that in figure 12 does not instantly reveal whether observed defects with strength ± 1 are line or point defects, both of which are possible. In order to distinguish between these two defect types in a general 3/3 dimensional simulation, a smaller lattice model (of $23 \times 23 \times 23$ cells) was used, again with equal elastic constants and free boundary conditions. Each of the 69 slices through the three orthogonal planes was plotted. The 'cores' of the defects were marked on each plot, enabling the cartesian coordinates of all the disclinations to be found and matched in three dimensions. An example is shown in figure 13 for three orthogonal slides chosen to intersect at a disclination observed at the point $x = 10$, $y = 15$, $z = 16$. The director trajectories about this defect reveal that the projection on to the z–x plane has the form of a radial $s = +1$ disclination, while the projections on to the y–z and x–y planes show $s = -1$ singularities. Combining these into a three dimensional structure leads to a point defect composed of $s = -1$ and $s = +1$ components as described by Demus and Richter [21]. An 'artist's impression' of such a defect is given in figure 14 (*a*). According to this model the z–x section in figure 13 (*c*) approximately corresponds to the 'equatorial plane' of the defect as shown in figure 14 (*d*) while x–y and y–z slices approximately correspond to the 'meridional planes' in figure 14 (*b*) and (*c*), respectively. Examination of the z–x slices above and below the central region of the defect supports the 3/3 dimensional picture, as the directors are observed to point progressively out of the plane on sections further from the defect, while still retaining their radial orientation as illustrated in figure 15. Similarly, at displacements along the x and/or z directions away from the meridional planes, the director field retains its $s = -1$ character.

Analysis of other disclinations in this model reveals a marked preponderance of point over line defects, with the majority of defects having point character. The development of microstructure as the simulation progresses appears to occur by the annihilation of pairs of point singularities of opposite strengths.

4.2.2. *Modelling of escape into the third dimension*

It is possible to envisage a mechanism by which + or −1 line defects decompose into a series of point singularities positioned along the original line. This mechanism has come to be known as 'escape into the third dimension' [22, 23] and is, of course, impossible for either a 2/2 or 2/3 dimensional system.

In order to simulate this process in as controlled a manner as possible, an $s = +1$, $\eta = 0$ disclination (ten layers thick) was generated using the Nehring–Saupe expression (14). The relaxation simulation was then run from this starting position (shown in figure 16), with the boundary orientations at the vertical edges of the stack fixed. It is apparent from figure 17 that as relaxation proceeds, the directors at the core of the disclinations reorient out of the plane normal to the original disclination line. Summation of the total energy of both the line and escaped configuration of the aggregate confirms that the escaped structure indeed has the lower energy.

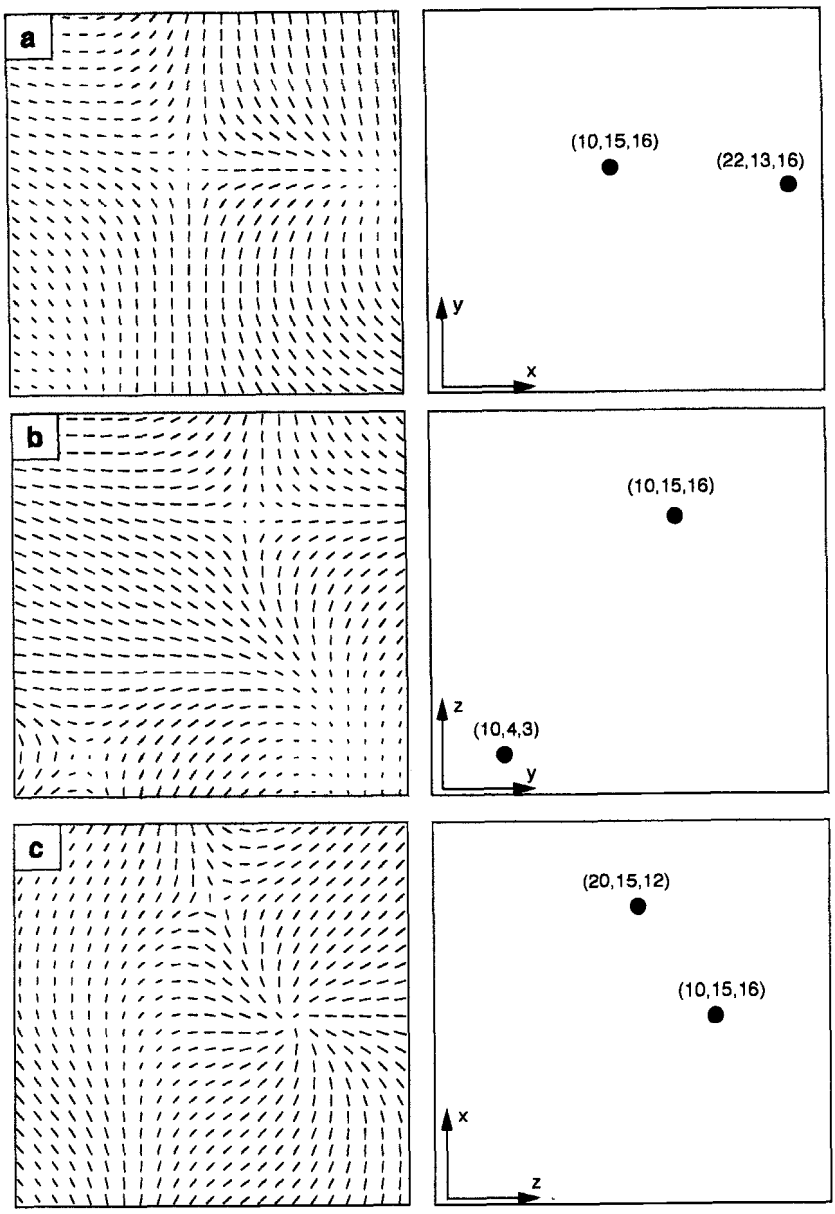

Figure 13. Slices through the (*a*) $z=16$ plane, (*b*) the $x=10$ plane and (*c*) the $y=15$ plane, together with disclination maps for a $23\times23\times23$ simulation using free boundary conditions and equal elastic constants. The figure shows three orthogonal projections of the defect passing through the point $x=10$, $y=15$, $z=16$.

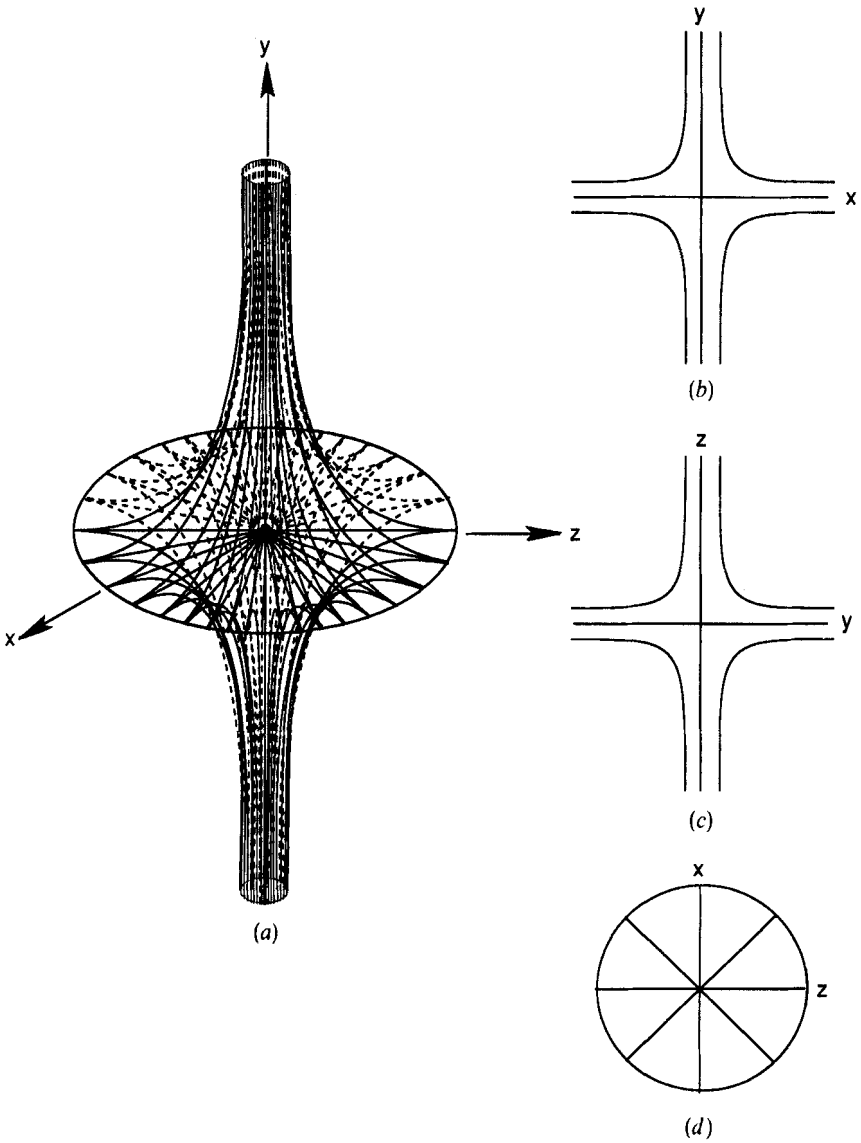

Figure 14. (*a*) Proposed model of the point defect which passes through the point $x = 10$, $y = 15$, $z = 16$. (*b*) A section of this defect on the x–y plane. This plane is an example of a 'meridional' section through the defect, (*c*) is the section on the y–z plane. Again this is an example of a 'meridional' section, (*d*) shows the z–x plane which is the 'equatorial' plane.

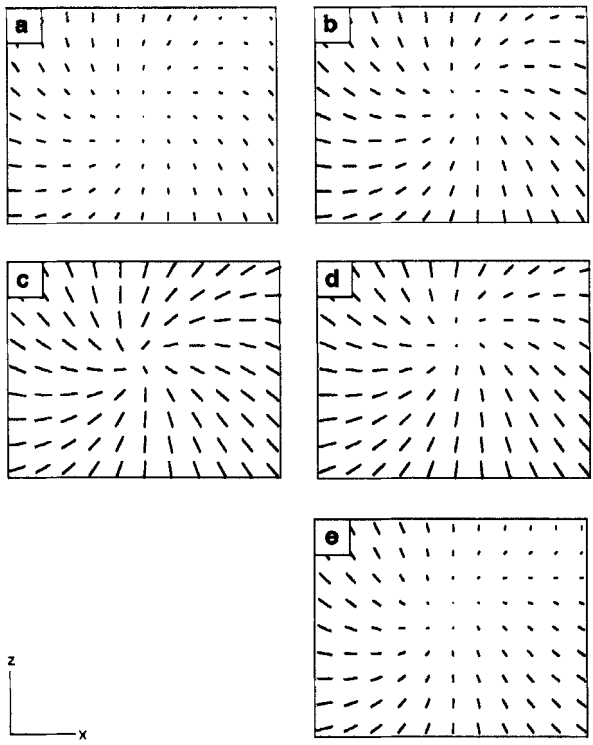

Figure 15. Enlarged z–x projections close to the core of the defect on the layers $y = 11, 13, 15, 17$ and 19, respectively from (*a*) to (*e*). The directors point progressively out of the plane on planes displaced further from the 'equator'. The equatorial section approximately corresponds to $y = 15$ (see (*c*)).

The core of the disclination can escape into both the positive or negative z direction with equal probability and examples of each are shown in figures 17(*b*) and (*c*). Therefore, in longer models (along the direction of the original line), $s = \pm 1$ point disclinations are formed along the axis of the stack as well as at the top and bottom surfaces. Despite the difference that the model is a square prism rather than a cylinder, such simulations mimic well the capillary tube experiments of Kléman and co-workers [23, 24] in which arrays of point disclinations were observed along the axis of thin capillary tubes, as shown in figure 18. This model is the only one considered so far which includes a free surface, and it has been calculated without involvement of the surface elastic constant, K_{24}. While such a modification may well have influenced the trajectories in the vicinity of the free surface, it does not detract from the demonstration that the current approach to modelling successfully predicts the phenomenon of escape in capillary tube type geometries.

The prediction of Kléman [2] that neither structures in which the splay and bend elastic constants are very different, nor those which have high bend energy, undergo escape, can be tested using the same configuration as above. The high bend energy case ($BE = 100$, $SP = TW = 1$) remains stable in the two dimensional splay rich 'star' starting configuration, indicating that $s = 1$ line defects are stable in 3/3 dimensions under these conditions. For high splay energy ($SP = 100$, $BE = TW = 1$), on the other hand, the star structure splits into two planar $s = \frac{1}{2}$ disclinations ('archways' which are rich in bend) with no out of plane perturbation, as shown in figure 19. The structure therefore

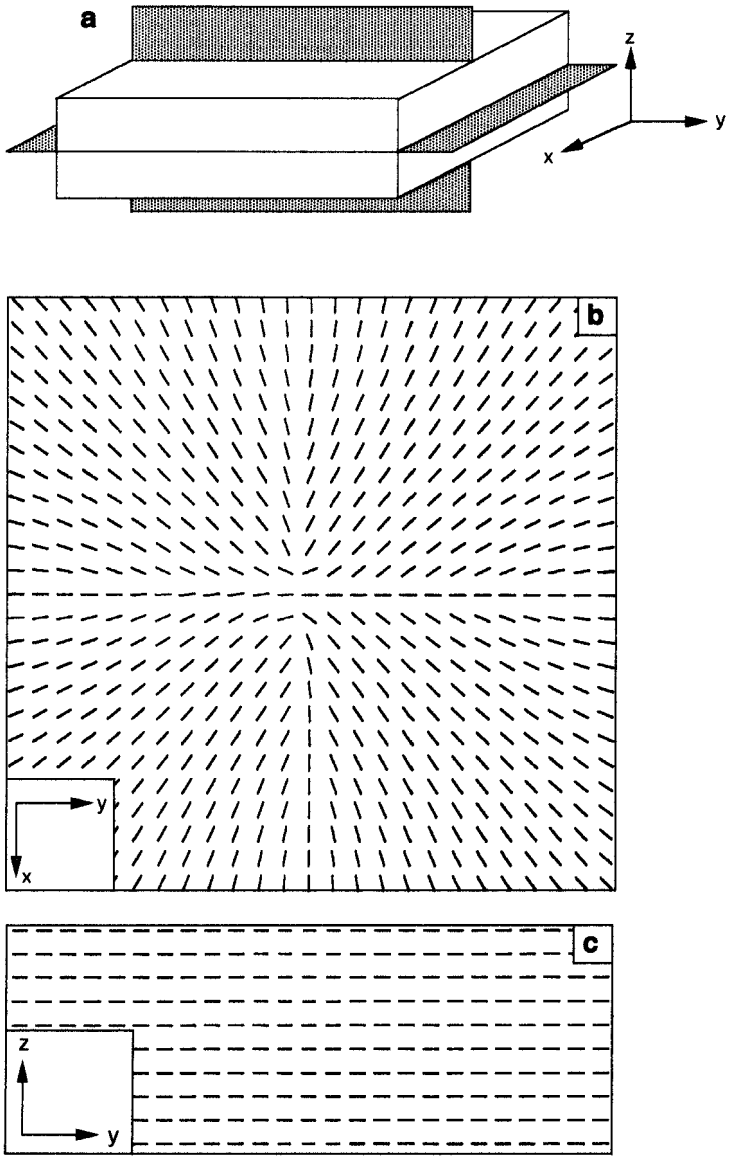

Figure 16. Starting configuration for the simulation of escape into the third dimension. (*a*) shows schematically the planes in (*b*) and (*c*): (*b*) is the defect as seen on the x–y plane and (*c*) the defect on the y–z plane at the position shown.

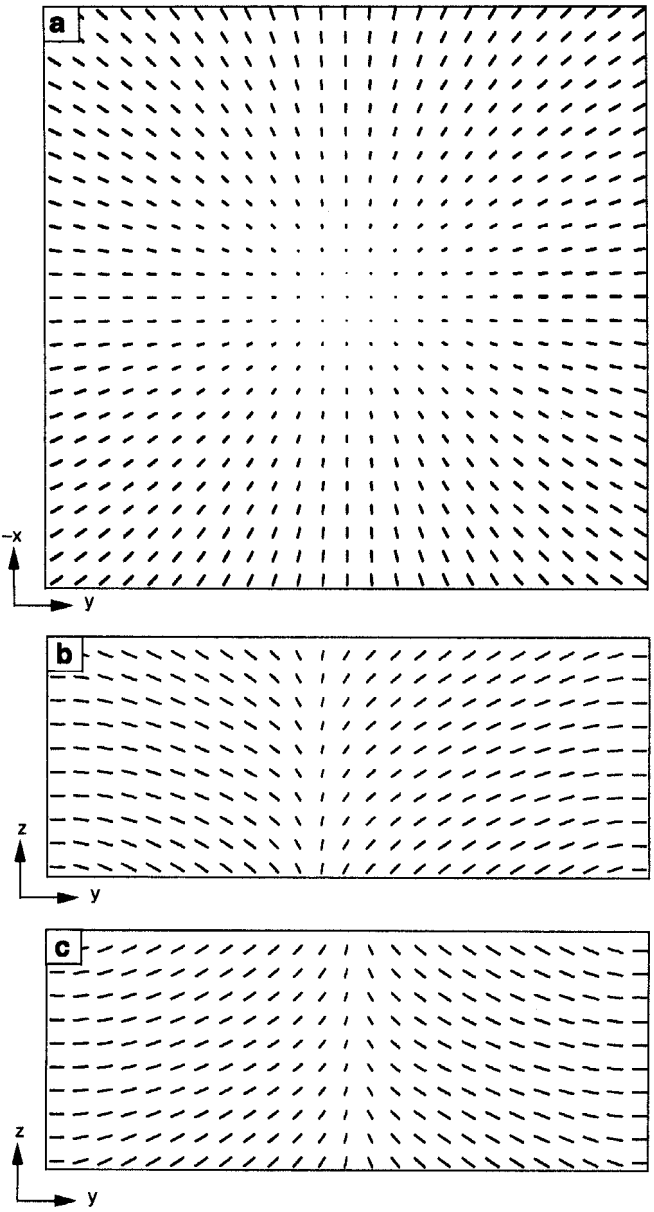

Figure 17. (*a*) The top (x–y) surface of an escaped $s = +1$ disclination simulated for $SP = BE = TW$ and fixed radial boundary conditions. The directors 'escape' out of the plane at the centre of the defect. Escape can occur in either the positive or negative z directions as shown in (*b*) and (*c*).

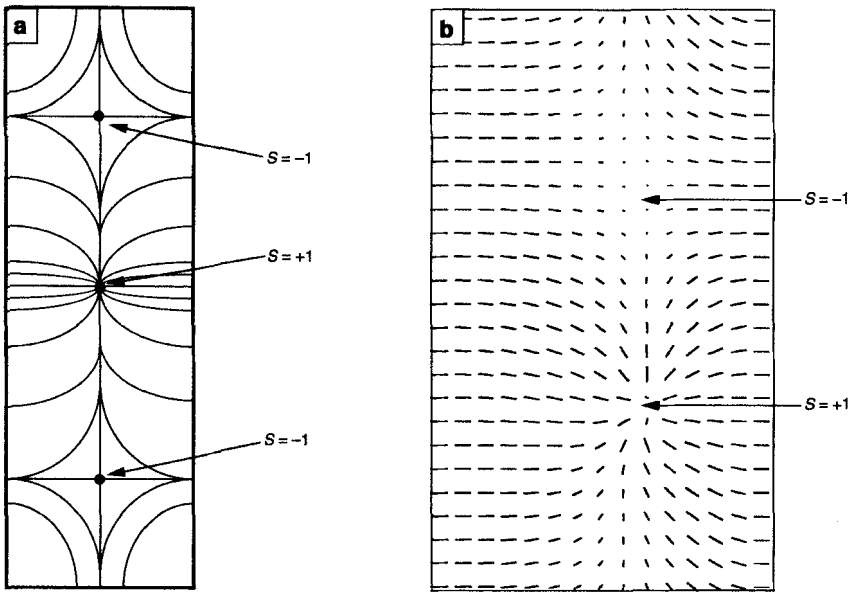

Figure 18. The central plane of point disclinations in a capillary tube; (*a*) shows the observed [23] and (*b*) the structure simulated with equal elastic constants and fixed radial boundary conditions.

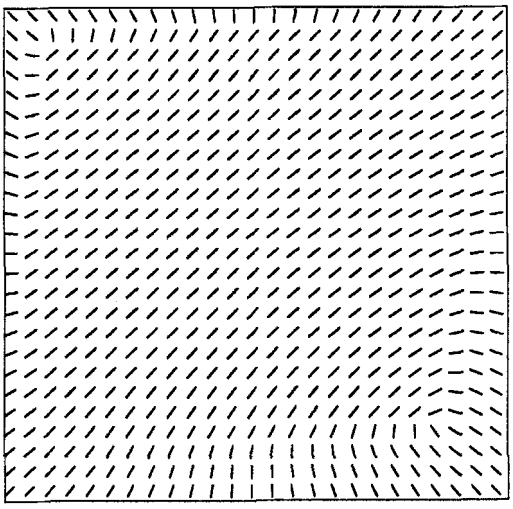

Figure 19. The x–y projection of the disclination in figure 17 having relaxed with fixed radial boundary conditions and elastic constants $SP=100$, $BE=1$ and $TW=1$. The structure does not undergo any deformation into the third dimension, but dissociates into two $s=\frac{1}{2}$ disclinations.

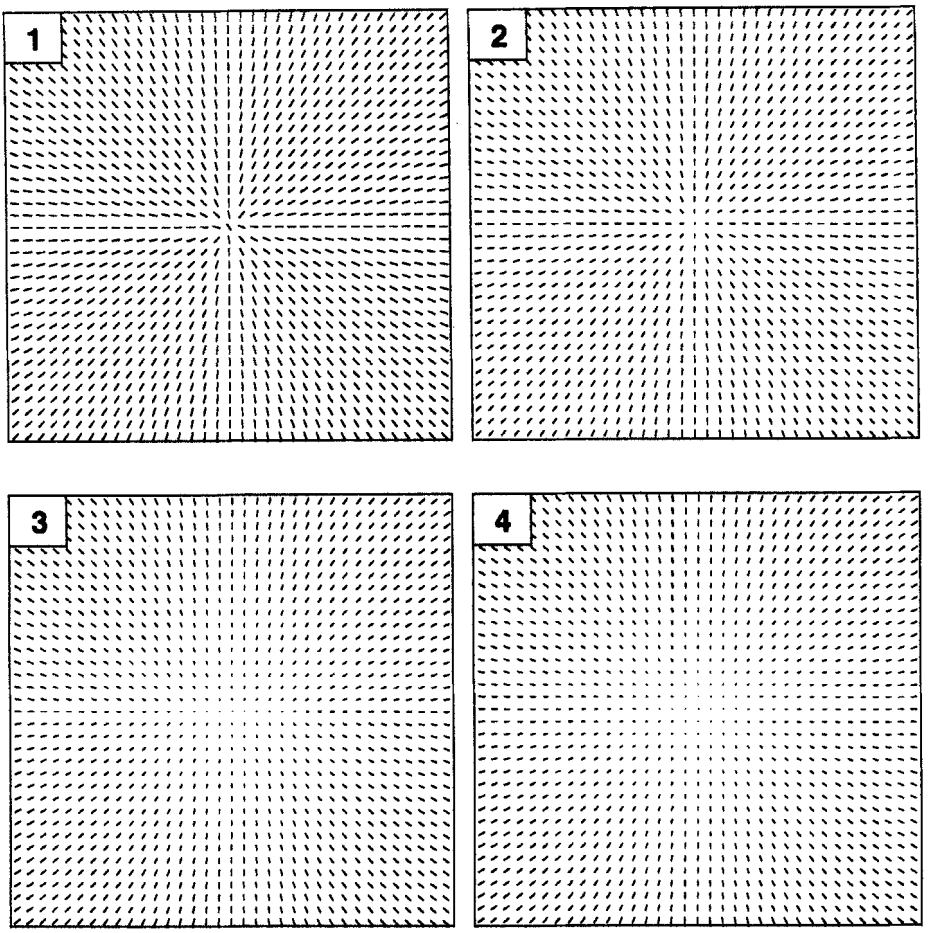

Figure 20. Sections through a radial $s=1$ point defect simulated with $SP=1$, $BE=100$ and $TW=1$.

minimizes splay in an analogous manner to the two dimensional case. This structure has been referred to as 'planar polar' by Allender *et al.* [25] in a paper in which its energy is compared with that of escaped structures as a function of the strength of boundary anchoring and the surface elastic constant K_{24}. Similar configurations have been observed in polymer liquid crystal display devices under conditions of high splay and appropriate anchoring energies [26], although in the case of the simulations using a square cross-sectioned lattice it should be noted that the $s=+\frac{1}{2}$ disclinations have a marked preference for the corners, presumably because in this way they can get further apart from each other.

4.2.3. *Stability of point defects for differing elastic constants*

Point defects are most usually observed in nematic droplets [27, 28] or at a nematic isotropic interface [29]. A radial (hedgehog [27]) point disclination can be stabilized on a $35 \times 35 \times 35$ lattice by fixing the orientation of the boundary cells to point radially inwards to the centre. This is the 3/3 dimensional analogue of the $s=1$ star disclination described in § 2. In order to favour the splay rich defect, the splay energy is set equal to that of twist, but with the bend energy 100 times greater. As expected, the point defect

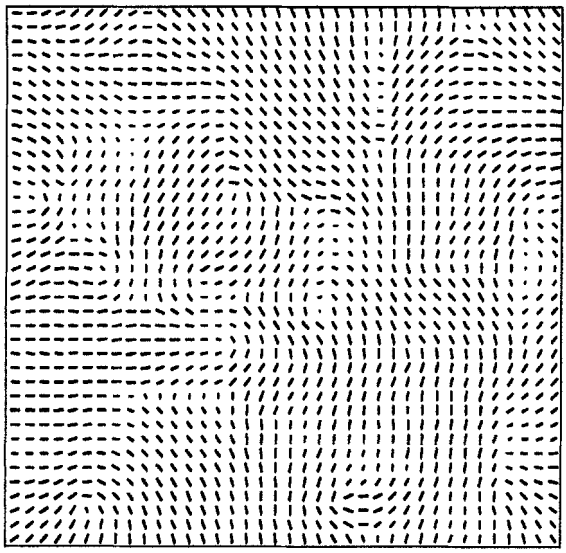

(*a*)

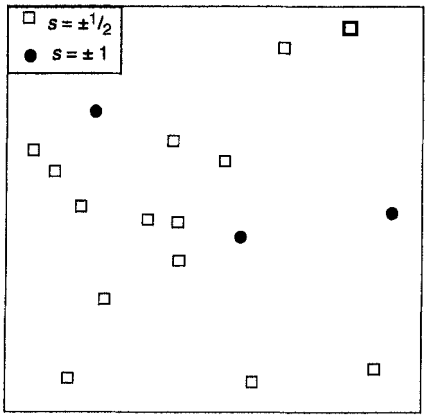

(*b*)

Figure 21. (*a*) An x–y slice through a 3/3 dimensional simulation using free boundary conditions and $SP=10$, $BE=1$ and $TW=1$. The simulation was terminated after approximately half the iterations required for a monodomain. More $s=\frac{1}{2}$ defects are observed than $s=1$ point defects because the higher splay energy means that escape into the third dimension is not energetically favourable. (*b*) The map showing the location of the integral and half integral defects.

forms readily and is shown as a series of sections of the x–y plane in figure 20. The defect is stable and undergoes no change when the boundary conditions are relaxed. Unlike the 2/2 dimensional case, the defect is also observed to be stable when the elastic constants are equal, as has been predicted from the continuum theory [27].

In a liquid crystalline polymer, the splay constant is thought to be much higher than that of either bend or twist [5]. In figure 21 a slice is shown through the x–y plane of a simulation using free boundary conditions in which the splay elastic constant is equal

to ten times that of bend and twist. In contrast to the case of equal elastic constants, there are now more $s = \pm\frac{1}{2}$ disclinations than $s = \pm 1$ point disclinations. This may be accounted for by the requirement of both bend and splay for this process to occur [2].

4.3. *Application of the model to the texture seen in thin films of high molecular weight polyesters*

In many of the situations to which the model has been applied, the splay, twist and bend energies have been equal and the modelling is thus more relevant to small molecule systems than polymers. However, the model appears to operate successfully in predicting known textures, and is also in agreement with analytical predictions of direct fields where these are available. The confidence thus acquired has led us to use it to address the long standing issue of the fine-scale textures observed in high molecular weight thermotropic copolyesters of the 'Vectra' type. We have previously [30] reported a series of microstructural observations which suggested that the fine-scale (so called 'tight') textures are disordered counterparts of the well-characterized banded texture, and that in each case the planar boundary conditions at the top and bottom surfaces of the sheet sample propagate through the polymer to produce a layer-like, fissile structure.

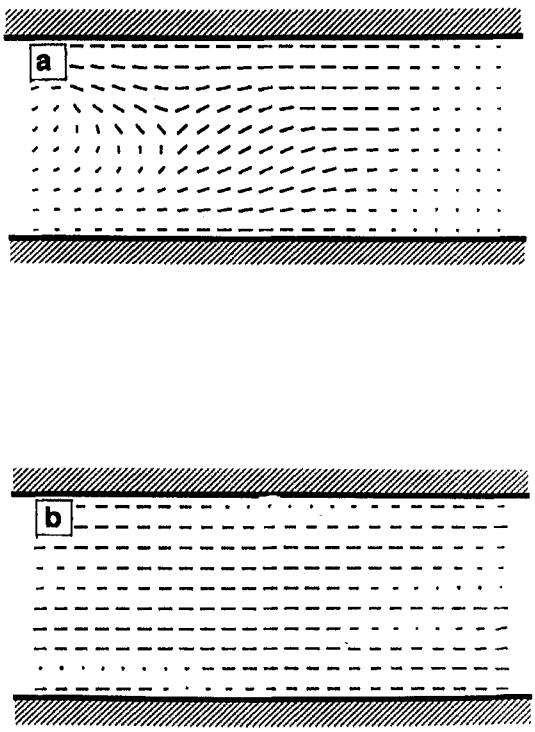

Figure 22. Edge-on views of two structures at equivalent stages of development with planar boundary conditions at the top and bottom surfaces of the diagram. In (*a*), the splay, twist and bend energies are set equal, while in (*b*) splay is set to be 100 times the energy of the other two distortions. The planar boundary conditions propagate to a much greater depth when splay is high.

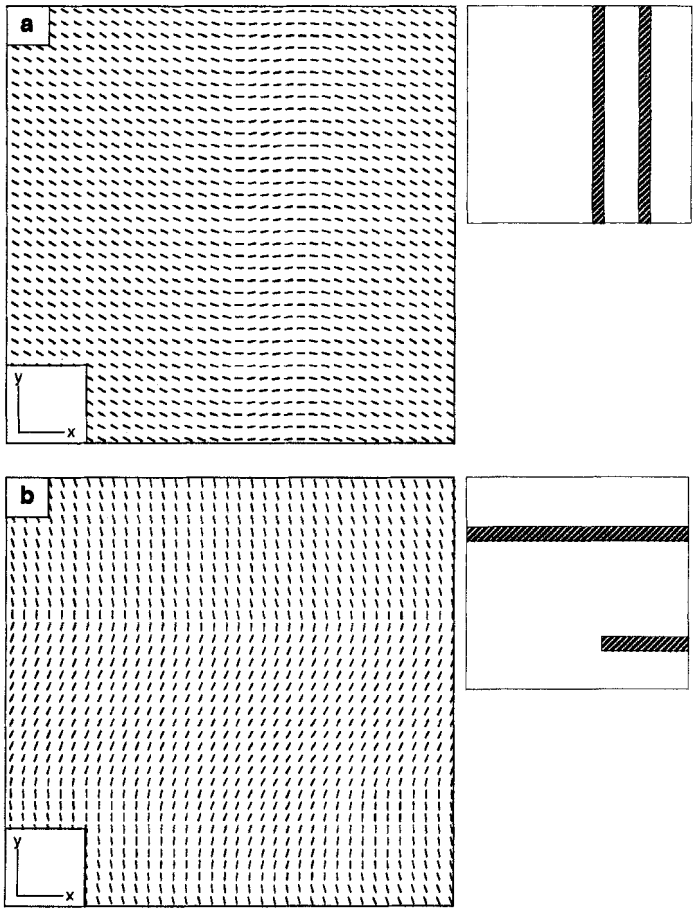

Figure 23. x–y Slices through successive layers of a 3/3 dimensional model simulated using the elastic constants $SP = 100$, $BE = 1$ and $TW = 1$ and terminated after approximately half the iterations required for a monodomain. Boundary conditions are planar on the top and bottom surfaces and periodic elsewhere. The structure forms a layered morphology in which there is little matching from layer to layer and a sinuous trajectory within the layers. The hatching in the inset diagrams shows regions which would appear dark if the structure was to be viewed through crossed polars orthogonal to the page.

Following an indication by Meyer [31] that, in cases where the splay energy is high such as with polymers, the splay component of deformation will be much more diffuse than either twist or bend, the propagation of planar boundary conditions was modelled for two limiting conditions: (i) equal distortion energies (splay = twist = bend); (ii) splay energy one hundred times that of bend and twist. These two simulations are shown in figure 22, each model having run for approximately the same number of cycles. It is clearly apparent that the planar surface orientation exerts its influence to a much greater depth in the specimen with the high splay energy. The lower bend and twist energies mean that monodomain order is not developed within the layers. Figure 23 shows examples of the structures which are developed in the layers, the lateral boundary conditions in this case being periodic. The x–y sections shown in (*a*) and (*b*) are neighbours in the stack but are observed to exhibit little matching with each other

since twist is set to be a low energy compared with splay. The structure may therefore be considered as fissile layers lying parallel to the top and bottom surfaces. Within the layers the directors are observed to follow sinuous trajectories containing regions of considerable bend, but only very gentle splay. This undulating structure is very reminiscent of the banded [32] and tight textures [3, 30] observed in thermotropic copolyesters, although it should be emphasized that the model makes no predictions with respect to the size-scale of the structure. The simulation has not yet been run with a preferred starting orientation commensurate with a shear axis, and thus long range, regular banded textures which must also involve through-thickness orientational correlation, have not yet been generated.

Nevertheless, the modelling developed so far indicates that the fissile nature of films of high molecular weight main chain thermotropics without flexible spacers is related to the occurrence of both tight and banded textures, and that all three features stem from the high splay distortion energies characteristic of these polymers.

5. Conclusions

(i) It is possible to simulate microstructures on two dimensional lattices that are in good agreement with those predicted by the continuum theory, both when the elastic constants are approximately equal, as in small molecule liquid crystals, and when they are very different, as is the case for liquid crystalline polymers. For example, the model correctly predicts that $s=-\frac{1}{2}$ disclinations have a morphology that does not appreciably alter as the ratio of the elastic constants is varied, while that of the $s=+\frac{1}{2}$ disclinations undergoes a marked change. There is close agreement between the trajectories of the simulated $s=+\frac{1}{2}$ disclinations and those calculated using the Nehring–Saupe expression for a variety of elastic constants.

(ii) $s=\pm 1$ disclinations, whose energies are four times that of the $s=\pm\frac{1}{2}$ disclinations are rarely seen in 2/2 dimensional simulations, unless favoured by both the ratio of the elastic constants and particular boundary conditions.

(iii) In 3/3 dimensional models simulated using equal elastic constants, the majority of disclinations are of type $s=\pm 1$, but are point disclinations in contrast to the 2/2 dimensional case. Point disclinations can be considered as the result of the process of escape into the third dimension.

(iv) 3/3 dimensional simulations performed with free boundary conditions, and with the splay energy set very much higher than that of bend or twist exhibit a predominance of $s=\pm\frac{1}{2}$ line disclinations, because escape into the third dimension is no longer favoured. Similar simulations performed with planar boundary conditions at the top and bottom surfaces produce layered microstructures with little correlation between the layers and a sinuous trajectory within the layers. This behaviour is seen as having key importance in the formation of both the banded and tight textures observed in liquid crystalline polymers, while also explaining why they are not observed in small molecule mesophases where the elastic constants are much more similar.

The simulations, which are in essence iterative steps in the solutions of Frank's equation by a finite difference approach, appear able to describe the evolution of the microstructures which are observed in real liquid crystal systems, both for small molecules and liquid crystalline polymers. The model is capable of further development in several ways such as the inclusion of shear and magnetic fields and the simulation of microstructure developed at finite temperatures.

We wish to thank ICI for providing a studentship and W. A. MacDonald, D. J. Blundell and T. M. Nicholson for helpful discussions during the course of this work.

References

[1] FRIEDEL, G., 1922, *Annln. Phys.*, **18,** 273.
[2] KLÉMAN, M., 1989, *Liq. Crystals*, **5,** 399.
[3] WINDLE, A. H., VINEY, C., GOLOMBOK, R., DONALD, A. M., and MITCHELL, G. R., 1985, *Faraday Discuss. chem. Soc.*, **79,** 55.
[4] GRAZIANO, D., and MACKLEY, M. R., 1984, *Molec. Crystals liq. Crystals*, **106,** 73.
[5] LEE, S. D., and MEYER, R. B., 1991, *Liquid Crystallinity in Polymers: Principles and Fundamental Applications*, edited by A. Ciferri (VCH), Chap. 9, p. 343.
[6] ZHENG-MIN, S., and KLÉMAN, M., 1984, *Molec. Crystals liq. Crystals*, **111,** 321.
[7] BEDFORD, S. E., NICHOLSON, T. M., and WINDLE, A. H., 1991, *Liq. Crystals*, **10,** 63.
[8] LEBWOHL, P. A., and LASHER, G., 1972, *Phys. Rev.* A, **6,** 426.
[9] ALLEN, M. P., and WILSON, M. R., 1989, *J. Comput. Aided Molec. Design*, **3,** 335.
[10] DENHAM, J. H., LUCKHURST, G. R., ZANNONI, C., and LEWIS, J., 1980, *Molec. Crystals liq. Crystals*, **60,** 185.
[11] KILIAN, A., and HESS, S., 1989, *Z. Naturf.* (*a*), **44,** 693.
[12] DE GENNES, P. G., 1974, *The Physics of Liquid Crystals* (Clarendon Press), Chap. 3, p. 65.
[13] FRANK, F. C., 1958, *Faraday Discuss. chem. Soc.*, **25,** 19.
[14] BEDFORD, S. E., 1992, Ph.D. Thesis, Cambridge University.
[15] ALLEN, M. P., and TILDESLEY, D. J., 1987, *Computer Simulation of Liquids* (Oxford Science Publications), Chap. 7, p. 212.
[16] NEHRING, J., and SAUPE, A., 1972, *J. chem. Soc. Faraday Trans. II*, **68,** 1.
[17] DZYALOSHINSKII, I. E., 1970, *Soviet Physics J.E.T.P.*, **31,** 733.
[18] HUDSON, S. D., and THOMAS, E. L., 1989, *Phys. Rev. Lett.*, **62,** 1993.
[19] NICHOLSON, T. M., 1989, *Molec. Crystals liq Crystals*, **177,** 163.
[20] MEYER, R. B., 1982, *Polymer Liquid Crystals*, edited by A. Ciferri, W. R. Krigbaum and R. B. Meyer (Academic Press), Chap. 6, p.133.
[21] DEMUS, D., and RICHTER, L., 1978, *Textures of Liquid Crystals* (Springer Verlag).
[22] CLADIS, P. E., and KLÉMAN, M., 1972, *J. de Physique.*, **33,** 591.
[23] MEYER, R. B., 1973, *Phil. Mag.*, **27,** 405.
[24] WILLIAMS, C. E., CLADIS, P. E., and PIERANSKI, E., 1973, *Phys. Rev. Lett.*, **29,** 290.
[25] ALLENDER, D. R., CRAWFORD, G. P., and DOANE, J. W., 1991, *Phys. Rev. Lett.*, **67,** 1442.
[26] DOANE, J. W., 1991, *M.R.S. Bulletin*, **16,** 22.
[27] CHANDRASEKHAR, S., and RANGANATH, G. S., 1986, *Adv. Phys.*, **35,** 507.
[28] PRESS, M. J., and ARROTT, A. S., 1975, *J. Phys., Paris*, **C1,** 178.
[29] MEYER, R. B., 1972, *Molec. Crystals liq. Crystals*, **16,** 355.
[30] BEDFORD, S. E., and WINDLE, A. H., 1990, *Polymer*, **31,** 616.
[31] MEYER, R. B., 1982, *Polymer Liquid Crystals*, edited by A. Ciferri, W. R. Krigbaum and R. B. Meyer (Academic Press), p. 151.
[32] DONALD, A. M., VINEY, C., and WINDLE, A. H., 1983, *Polymer*, **24,** 155.